THE UNIVERSITY of ADELAIDE

The Mound Springs of South Australia: Their Electromagnetic Signature and Fractal Dimension

Katherine Stoate
Submitted for B.Sc. (Honours)

Supervisors: Graham Heinson & Mike Hatch

University of Adelaide
North Terrace, Adelaide, S.A.
katherine.stoate@student.adelaide.edu.au
October 24th 2011

Abstract

The importance of groundwater to remote and regional Australia cannot be understated, due to the intermittent and unreliable rainfall in these areas, as well as the unreliability of other water sources. As such the major source of water is groundwater from the Great Artesian Basin (GAB). The natural discharge of the GAB is through mound springs, unique landforms comprised of precipitated carbonates that are primarily located along the south western edge of the GAB. Due to the cultural, economic and environmental significance of these features it is important to fully understand their underlying hydrogeological structure. Geophysical studies have the potential to provide non-invasive imaging of these specific aspects of the GAB. A number of different methods were used to collect data from the springs. For this particular study a set of shallow electromagnetic data was collected. These data were processed conventionally, however to provide additional information they were also processed to extract the fractal dimension information of the data. The fractal dimension is used here as an indicator of roughness or texture with a dataset, thus differentiating between a homogenous and heterogeneous earth. All of the data were compared, including conductivity, in-phase, fractal dimension and the regolith of the area. It was hoped that this would provide added depth to the understanding of the mound springs as well as trialling an alternate method of processing data. Although the data collected did show some correlations, especially in regards to the relationships between the conductivity and the EM signature of the mound springs, there was a lack of consistent correlation between the fractal dimension and the other data sets that did not allow for conclusions as to the usefulness of fractal dimension as a means of processing data. This may be due to the small survey size of the area, thus testing on larger areas may be worthwhile in the future.

Keywords: Mound Springs, Great Artesian Basin, EM surveys, Fractal Dimension, Regolith.

Table of Contents

Introduction

The importance of groundwater to remote and regional Australia cannot be understated. Since inland Australia receives intermittent rainfall and evaporation rates are extremely high, directly collected rainwater and water sources such as dams and creeks are not reliable. As such, communities and industry must rely on water sourced from the subsurface. The major source of groundwater in inland Australia is the Great Artesian Basin (GAB), which covers ~22% of the continent (Habermehl 1980). A form of natural discharge for the GAB is the mound springs that are found along the south western margin (Figure 1). Both the springs, as well as bores into the GAB, have supported regional communities since the 1920s, and this has lead to a decrease in the flow from the springs and a lowering of the potentiometric surface (Habermehl 1982). The springs are also of major cultural significance to the local Indigenous communities. Given the cultural, economic and environmental importance of the mound springs to the region it is important that the mechanisms that control the springs are well understood and the effect that these mechanisms have on the GAB are continually monitored. The use of different Geophysical methods has the potential to provide non-intrusive imaging of the subsurface as well as assist in monitoring of groundwater levels and flow paths (McNeill 1980; Burger 2006).

In this study, a number of different geophysical techniques were used to better understand the GAB, the mound springs and the movement of groundwater. These include shallow frequency domain electromagnetic (EM), spectral induced polarisation (IP), high resolution transient electromagnetic (TEM) and self potential (SP). This study concentrates on the frequency domain EM, focusing particularly on how the data are processed and imaged. Specifically this thesis examines whether the “texture” of the data as seen by the means of processing using the fractal dimension adds information that is missed by examination and interpretation of the conductivity data alone.

Fractal dimension can be said to be a measure of the roughness or texture of a data (Mandelbrot 1977; Turcotte 1997). A fractal is a scale invariant object or dataset which is characterised by its underlying statistics being similar at all scales (Mandelbrot 1977; Turcotte 1997). In this study fractal dimension is based on an analysis of the power spectrum.

Fractal dimension has been used in geology and geophysics as a means to model fracture networks both at a regional and continental scale, to investigate geomorphology and for applications specific to mining and ore production (Chilès 1988; Turcotte 1989; Andrle 1992; Turcotte 1997). Fractal dimension has also been used to model fluid flow and connectivity within porous and fractured media (Adler & Thovert 1993; Renshaw 1998). Everett and Weiss (2002), show that the geological signal within a data set collected using an electromagnetic instrument from the subsurface is likely to be fractal in nature, and is the basis for this study. Studies conducted by Tania Dhu (2003; 2004b) also form the basis of this work, with a continuation of the comparison between conductivity, fractal dimension and regolith.

As the frequency domain EM data that were collected concentrates on the shallow subsurface, a regolith map was used as another data set with which the results can be compared. This map was compiled from field observations, and includes all of the area that was covered by the EM survey.

Background

The Great Artesian Basin: Geology and Hydrogeology

The GAB covers 22% of the Australian continent, and is an integral part of human settlement in the remote regions of inland Australia (Habermehl 1980; Harris 1997; Cox 1998). The recharge areas are found along the eastern edge of the basin, with the majority of flow proceeding to the southwest with most discharge at the south western edges of the basin (Figure 1). Basin discharge occurs from natural springs and seeps as well as a number of anthropogenic bores (Habermehl 1980; Aldam 1988; Mudd 2000).

The geology of the GAB is comprised of confined groundwater basins with aquifers of sandstone and confining beds of marine mud and siltstone (Habermehl 1980; Habermehl 1982). The basin is up to 3000m thick in some areas and forms a large synclinal structure which, due to uplift, has exposed the eastern margin (Figure 2; Habermehl 1980). The majority of the recharge areas of the basin are situated along this eastern edge at the Great Dividing Range, while discharge occurs to the southwest (Williams & Holmes 1978; Habermehl 1980; Habermehl 1982).

Large scale fault and fold systems are present through the basin, however it is the small scale faults that are more significant in terms of this study (Habermehl 1982; Cox 1998). These local faults and folding provide connection between separate aquifers and act as preferential paths for groundwater movement (Figure 3; Habermehl 1982).

The aquifers that are of most interest are the Cadna-owie formation and the Hooray Sandstone, with most aquifers being continuous and hydraulically connected across the geological basin (Habermehl 1980; Love 2008). Tertiary and Quaternary lithologies also contain aquifers, which are widely but not continuously distributed across the basin, and therefore are not considered part of the GAB (Habermehl 1980). The Cadna-owie formation is generally less than 20m thick in the south western margins where it is exposed, and up to 70m thick in other areas of the basin (Tyler 1990).

The Bulldog Shale is the main confining bed of interest in this region, and is part of the Marree subgroup, which can be up to 750m thick (Tyler 1990) and overlies the Cadna-owie group. The Bulldog Shale is a shaly mudstone with silty, fine sand and limestone phases (Tyler 1990).

The hydrogeological basement is Pre-Jurassic, and where the sequence is complete, is the Rewan Group (Habermehl 1980). The aquifers of the GAB are generally separated from the higher salinity groundwater contained within older Permian units, except in the southwest of the basin, where Permo-Triassic material is in direct contact with Jurassic aquifers (Habermehl 1980).

The Mound Springs of the Lake Eyre Region:

The artesian springs which are found in the Lake Eyre region differ from "normal" artesian springs, as the ground water brought up has high levels of clay and sand, while calcium carbonate within the groundwater is precipitated by algae and bacteria (Herczeg *et al.* 1991; Prescott & Habermehl 2008). These concentrate and precipitate on the margins of the springs over time, creating a significant 'mound' feature in the landscape (Habermehl 2001; Prescott & Habermehl 2008). Eventually these mounds become large enough that the artesian head pressure is balanced by the height of the mound, and the spring no longer flows (Habermehl 2001; Keppel 2011). Artesian springs are generally thought of as being the result of 3 different scenarios: 1) Faults along which the water flows upwards; 2) The abutment of aquifers in the sedimentary sequence against impervious bedrock; and 3) From pressurised water breaking through thin confining beds near the discharge margins of the basin (Habermehl 1980, 2001)

Mound springs are typically comprised of a central carbonate mound, with outer zones dominated by sulphate and chlorite salts (Habermehl 2001; Prescott & Habermehl 2008; Keppel 2011). Discharge rates from the systems are controlled by hydrochemistry, evaporation, organic and inorganic carbonate precipitation, local subsidence and micro tectonics (Habermehl 2001; Love 2008; Keppel 2011). Mound springs in the south-western margin are dominated by calcite, dolomite

and a fine grained carbonate precipitate, deposited from the groundwater (Habermehl 2001; Love 2008; Keppel 2011). Within the landscape of the Lake Eyre region, the older springs are topographically higher than the younger springs. Much of the height difference between old and new springs may be a result of the lowering of the land surface and spring outlet levels during the Quaternary (Habermehl 1980, 2001).

Geology of the Wabma Kadarbu

Wabma Kadarbu National Park, where field work took place, is situated approximately 100km north west of Marree (Figure 4). It contains a number of springs, both active and extinct and the geology and regolith are relatively complex. The local geology is dominated by Cretaceous age Bulldog Shale at or near the surface which appears to be outcropping across much of the area (Krieg 1992). Overlying the Bulldog Shale are mound spring deposits. The younger deposits are comprised of limestone and reworked Mesozoic sediments, formed during the Mid-Pleistocene. The older mound springs deposits, comprised of yellow-grey limestone, are of Pliocene age (Krieg 1992). Areas of Holocene aeolian sand dunes and Middle Pleistocene Telford gravel formation outcrop to the edges of the main study area (Krieg 1992).

Methodology

Electromagnetic Surveys

This survey uses a GF Instruments CMD-4 electromagnetic (EM), a highly portable hand held EM conductivity meter (Figure 5). This instrument is primarily sensitive to variations in the electrical properties of subsurface materials, and therefore may be used to differentiate higher conductivity regions from lower conductivity regions. (Munday 2009). The propagation of magnetic fields are generated by passing an alternating current through a loop or coil, which is positioned on the ground or in the air (Munday 2009). A secondary field is induced in the ground which is inductively detected in a receiver coil (Munday 2009). The strength of the secondary field is directly proportional to variations in conductivity in the subsurface (McNeill 1980).

The instrument uses Low Induction Number (LIN) approximation to estimate conductivity. The conductivity is based on the out of phase component of the measured data. For this type of instrument the in-phase component is often interpreted as a measure of the relative quantity of the primary magnetic field, closely related to the magnetic susceptibility of the measured material. The in-phase is suggested as a good indication of artificial metals objects, such as pipes and cables, and is recorded in parts per thousand, while the conductivity records in mS/m (G.F. Instruments ; McNeill 1980; Munday 2009).

Conductive materials produce strong secondary EM fields, while resistive units produce weaker secondary EM fields. Clays, saprolites and materials that are saturated by saline groundwater will generate stronger fields, appearing as conductors. Materials that are dry, sands and those that are saturated with less ionised water will appear as resistive (McNeill 1980).

It is important to note that these variations in the EM survey are not necessarily indicative of a particular material, as even classified signatures of materials have a great deal of variation (Munday 2009). This may be due to the relative saturation of the materials, or other factors such as

the percentage of clays to sand, which makes it difficult to determine an absolute classification of materials. Rather it is the spatial comparison of relative conductivities that gives the information about the area (McNeill 1980).

Due to the geometry and frequency range of EM instruments, the depth of investigation is usually in the range of three to six metres. For this particular instrument, the range has been established at approximately 6m, but the highest degree of sensitivity is at the surface (G.F. Instruments).

Electro-Magnetic Survey: Survey description

The EM data used for this study were collected using the GF Instruments CMD-4 (Figure 5). Positional information was collected using a differential GPS system and Fugro's Omnistar service with accuracy to less than 1m horizontally. The CMD-4 was set up to record positional information directly from the GPS.

The portable system and subsequent rapid acquisition of data, as well as minimal ground disturbance, were primary factors in determining that this system would be suitable for covering a large part of the survey area efficiently. Ultimately, this extensive coverage of the survey area was needed in order to perform the spatial analysis that was the aim of this project. Furthermore it was important that the survey impact was low, due to the cultural and environmental sensitivity of the area.

Initially, data were collected over three lines, labelled A, B and C (Figure 6). Line A is approximately 900m long and is orientated approximately north-south. Line B is also approximately 900m long, running from the southeast corner of the survey area to the northeast, and includes The Bubbler spring system. Line C is approximately 2km long, running from the northeast to southwest corner, and includes Blanche Cup, the other major spring in the survey area. Eight additional fill in

lines were collected at 100m intervals, running east-west across a portion of the survey area that contained the majority of the points of interest within the survey area.

Fractals, Fractal Dimension and the Power Law Spectra

In a practical sense fractals are sets of data that are self similar, such that they contain patterns within the data and their underlying statistics that are similar at all scales (Mandelbrot 1977; Turcotte 1997). The fractal dimension is a method of quantifying the complexity of that shape, and can also be seen as a measure of the roughness of the data set (Turcotte 1997).

There are three broad types of fractal dimension: geometric; stochastic; and spectral (Carr & Benzer 1991). Geometric, or deterministic, classification methods measure the complexity of the shape as a function of scale and the information comes directly from the data set (Turcotte 1997). Both stochastic and spectral classification types are achieved through statistical methods. Stochastic classification is based on the assumption that the data is a realisation of a statistical function, such as Brownian motion (Turcotte 1997). Spectral methods use the wave number or spatial frequency of a dataset to calculate the fractal dimension, which is achieved through the use of the power spectral density (Carr & Benzer 1991; Turcotte 1997; Dhu 2008).

A deterministic fractal set, or fractal distribution, is defined by Turcotte (1997) as the number of objects (N) with characteristic size greater than (r) scale with the relation $N \sim r^{-D}$, where (D) is the fractal dimension. Deterministic fractals are scale invariant and as such are similar at different scales (Turcotte 1989).

A deterministic fractal set, containing discrete values, is defined by the following:

$$N_i = \frac{C}{{r_i}^D} \qquad \text{Equation 1}$$

Where N_i equals the number of objects, C is the constant of proportionality, r_i is the characteristic linear dimension and D equals the fractal dimension (Turcotte 1997).

Alternatively, fractal concepts can also be applied to a statistical, stochastic, distribution:

$$N = \frac{C}{r^D} \qquad \text{Equation 2}$$

Where number of objects, *N*, with a characteristic linear dimension greater than *r*, need to satisfy the above relationship (Turcotte 1997). D is again the fractal dimension, and Equation 2 is primarily used for when the dataset is continuous, rather than being made up of discrete data points (Turcotte 1997).

The mathematical representations in Equations 1 and 2 are theoretically valid over an infinite range. However for any physical application of the fractal dimension there will be upper and lower limits on the applicability of the fractal dimension (Turcotte 1997). If scale invariance extends over a sufficient range of length the fractal distribution provides a useful description of the applicable statistical distribution (Turcotte 1997).

Spectral methods of classifying a fractal dataset is prominent within Turcotte's work (1997) and has subsequently been used by Carr and Benzer, (2001) and by Dhu (2008). A spectral fractal set is determined by the parameters of the underlying statistical function using spectral methods. There is a distinction between self affine and self similar fractal sets. A self similar fractal set is isotropic; it does not depend on the geometrical orientation of the x and y axes (Turcotte 1997). A self affine fractal set is not isotropic, and can be scaled by different amount in the x and y axes (Mandelbrot 1985; Turcotte 1997), in this study equations for self affine fractals have been used. Important to self affine sets is the Hausdorff dimension (Ha), which is the power law scaling of a self affine fractal. The relationship between the fractal dimension (D) and the Hausdorff dimension is defined by:

$$Ha = 2 - D \qquad \text{Equation 3}$$

For a self affine time series, the power spectral density (S) has a power law dependence on frequency characterised by:

$$S(f) \sim f^{-\beta}$$ Equation 4

where $S(f)$ is a function of frequency and β is the power law exponent.

From equations 3 and 4 it is possible to obtain a relationship between the Hausdorff dimension Ha, the power law exponent β and the fractal dimension D, which can be expressed as:

$$\beta = 2Ha + 1 = 5 - 2D$$ Equation 5

Which is then rearranged to the equation used by Carr and Benzer (1991):

$$D = \frac{5 - |\text{slope}|}{2}$$ Equation 6

In Equation 6, the $|\text{slope}|$ term is the same as β in Equation 5, and is the slope of the power spectrum.

The power spectrum is a plot of a given signal's power, expressed in energy per unit of wavelength or wave number (Weisstein 2011). The most common way to produce a power spectrum is through the use of a Fast Fourier Transform (FFT) (Weisstein 2011). The power spectrum can also be described as showing the strength of the variation of energy as a function of the frequency (Press 1992). Thus showing at what frequency the energy within the signal is strong or weak, in the units of energy per unit of frequency (Press 1992). The power spectral density (PSD) is found through using a FFT and is a useful tool in identifying oscillatory signals in time series data, if the amplitude is the parameter that is wished to be found (Press 1992). The power spectral density is also widely used to characterise random processes, such as noise, in a system (Howard 2003). From this characterisation the noise power and thus the signal to noise ratio can be determined (Howard 2003). The FFT is a means of defining the power spectral density, through decomposition of the signals that make up the random process (Howard 2003).

As previously mentioned the slope of the power spectrum is needed in order to calculate the fractal dimension. From Carr and Benzer (1991), the following means of estimating the power spectra are used:

$$P = P\left(f_{(0)}\right) = \frac{|C_0|^2}{N^2} \qquad \text{Equation 7}$$

$$P(f_k) = N^{-2}[|C_k|^2 + |C_{N-k}|^2], \qquad k = 1, 2, \dots, \left(\frac{N}{2} - 1\right) \qquad \text{Equation 8}$$

Equation 7 is the power defined at 0 frequency, while Equation 8 is a means of finding the power spectra for all other discrete frequencies.

Everett and Weiss (2002) suggest that the EM response of the subsurface is not uniform, with random noise imposed by geological structures (Everett & Weiss 2002). These authors state that subsurface conductivity variation is a function of the dimension or scale length, and that this dependence is fractal (Everett & Weiss 2002). This has the potential to provide additional information that may be useful in the interpretation of conductivity data.

The spectral form of fractal dimension, calculated from power spectral density (PSD) plots, can be used to differentiate between EM responses of different lithologies (Figure 7). The fractal dimension for a one dimensional profile is expected to lie within 1<D<2 (Fox 1989), although two dimensional profiles can have values >2. When the fractal dimension is below one, the conductivity variation is random and Gaussian. Alternatively values between 1 and 2 are considered to be non-Gaussian and as such have a spatial correlation (Dhu *et al.* 2004a). Therefore, conductivity variation that is shown to be Gaussian is likely to reflect well sorted, statistically homogeneous materials, while non-Gaussian will reflect heterogeneous material (Dhu *et al.* 2004a). Higher values of fractal dimension are held to correlate with long wavelength features within the signal, which in turn is held to relate to deeper signals within the subsurface (Dhu *et al.* 2004a).

Data Processing of the Fractal Dimension

As part of processing the data was re-sampled and interpolated linearly to intervals of 2m (Figure 8). This was done to regularise the distance between data points for the power spectra processing. A power spectra was then determined, with a fixed window size of 64 data points,

equating to 128m. For each re-sampled line there were N samples, spanning 2m. Starting from the 32nd sample, a power spectrum was calculated from the samples in the interval [1, 64]. Then for the 33rd sample, the power spectrum is calculated from samples in interval [2, 65], and so on until the sample at N-32, where the interval [N-64, N] is used. This results in N-64 power spectra (Figure 9a). As the data is in a spatial format not temporal, the frequency is produced is displayed in wave number (1/λ).

The slope of the power spectra was calculated by taking the gradient of the log of the power spectrum against the log of the frequency, or in this case the wave number. The fractal dimension, D, is estimated from the slope using Equation 6. As the log (power) is not exactly a linear function of log (wave number) it is necessary to estimate the slope by fitting a straight line to the data by minimizing the sum of the squared residuals. Error bars have also been calculated. In this study error bars are shown equal to two standard deviations (Figure 9b).

The resulting data set was then smoothed, as D is estimated every 2m, from a power spectrum that spans 64m in both directions by running a nine point moving average filter in both directions.

Other Data Processing

ArcGIS and Regolith Map

High resolution maps from Google Earth were georeferenced within ArcGIS, which allowed for the data to be spatially referenced. The data plotted up onto these maps included the conductivity and in-phase data and the fractal dimension.

A regolith map was produced using GIS software, with field observations and interpretation of the aerial photographs that are available from Google Earth. This was done because the CMD-4 characterises approximately the top 5-6m of the subsurface (G.F. Instruments), with the view that the regolith would closely correlate the data collected from the CMD-4.

Results

Conductivity and Inphase

The data collected from the CMD-4, includes both an in-phase component and an out of phase (conductivity) component.

The conductivity was plotted in ArcGIS against Google Earth images of the area which allows for highs and lows to be compared to what features of the landscape they correlate with (Figure 10). It can be seen in this figure that the springs, both active and extinct, correlate with areas of low conductivity. There seems to be no other consistent correlation, as areas that are expected to be conductive due to a covering of salt or the presence of moisture, were not. The elevation at which the conductivity measurements were taken, gained through the use of a differential GPS, were compared to the conductivity, again overlaid on a Google Earth image (Figure 11). Examination of this figure suggests that there is little or no correlation between elevation and conductivity. This figure did not reveal anything significant about the landscape. The landscape itself is relatively flat, with the highest points being the springs, generally $\leq$ 15m above the landscape, while the lowest points were in alluvial channels. A contour map of the conductivity was also produced (Figure 12), with the same results as what has been plotted just as data points. The springs have a significant low conductive response.

The in-phase is the second parameter measured by the CMD-4. In-phase is defined as the relative quantity, in parts per thousand (ppt), of primary magnetic field (GF Instruments ; McNeill 1980). This is closely related to the magnetic susceptibility of the measured material (GF Instruments ; McNeill 1980). The results from the in-phase tended to follow what was produced by the conductivity; there was less noise within the in-phase signal (Figure 13). Due to the relative lack of metallic objects within the survey area, especially those that would be buried, the inphase did not provide any information not seen in the conductivity data. Nevertheless both sets of data were

affected by the presence of metallic fence lines and to some extent the road. The fences predictably resulted in extremely high conductivity, and this was obvious when the conductivity was plotted using GIS software, as such these points were removed, as they produced false highs within the data set. The road had some effect on the conductivity, with a slight rise in conductivity in some areas, but this is not overly noticeable, nor does it overtly and consistently affect the data. These points were not removed from the data set.

Fractal Dimension

Along line fractal dimension results were plotted using GIS software in the same way as the conductivity data (Figure 14). As with the conductivity there seems to be no direct correlation between the fractal dimension and the landscape features in the survey area. The springs do show some correlation, but not all of the springs have the same fractal dimension signature.

Contour maps of the fractal dimension were also produced at 5m, 25m and 50m plotting intervals. The 5m image shows a better resolution of variations in the data over the area (Figure 15), while the 25m and 50m intervals may indicate different trends within the data, but these were not immediately obvious and were not looked at closely as a part of this study.

Regolith – Landform Map

The landscape and regolith of the survey area is dominated by mound springs, both active and extinct, and alluvial landforms. There are also areas around the springs, which have a build up of aeolian sands, as well as area between the springs that have been classified as colluvial plains and other landforms. The survey area has been subdivided and characterised with regolith landform unit codes.

A table of regolith landform unit codes is presented in the appendix as well as a full legend to the regolith landform map (Figures 16,17). Generalised classification is summarised in the following sections.

Transported Regolith

Evaporites (E)

The springs of the survey area have been classified as evaporites, with three different landforms; erosional rises *(er)* and mound spring *(mo*). The mound spring classification indicates an active spring system, while the class of erosional rises represent an extinct spring. The erosional rises are differentiated into two zones, one of which contains no vegetation, while the other does. The evaporites form topographical high points in the landscape, with the extinct springs dominating the western and southern margins of the survey area. Active springs are more concentrated to the central and northern part of the survey area.

Alluvial Sediments (A, AC)

The other major landscape features in the survey area are the alluvial channels, which are dominated by a) surface runoff, or b) spring runoff. Surface runoff features tend to trend east-west while spring runoff trends north-south. The landforms of the alluvial units include: alluvial plains *(ap)*, alluvial channels *(ah)*, floodplains *(af*), alluvial landforms *(a)*, drainage depressions *(ed)* and alluvial swamps *(aw).* These landforms dominate the areas between the springs, and are of generally lower elevation than the surrounding areas, hence the preferential path for surface runoff.

Aeolian Sediments (IS)

Zones of aeolian sediments have built up around the active springs, these have been assigned the landform unit code of sand plain *(ps)*. The other area of aeolian sediment build up is to the east of the survey area, on the other side of The Bubbler runoff, this also has the landform unit code of sand plain *(ps)*. These zones contain the majority of the vegetation that is found in the area, consisting of small shrubs, mainly blue and salt bush.

Colluvial Sediments (CH)

Colluvial sediments are found within the survey area; the landform units include playa plain *(pp),* erosional rise *(er)* and erosional plain *(ep).* These zones are situated along the flat areas between the channels and springs, and have a variable clay and sand composition. Generally these playa plains are not vegetated, whilst the erosional plains or erosional rises have some reeds and small (<1m) bushes. Some areas contain clasts of transported material, while the majority is characterised by salt precipitation on the surface.

Man-made/Anthropogenic

Dirt road/track into the National Park and the car parks at The Bubbler and Blanche Cup are the main anthropogenic effects in the area.

Comparative Datasets

Conductivity and Fractal Dimension

The conductivity and fractal dimension were graphed and plotted against one another (Figure 19, 20). Comparison of the results was variable, with some parts of lines showing a correlation between the fractal dimension and the conductivity. In other lines a reverse correlation was observed whilst some lines showed no correlation at all.

Conductivity and Regolith

In Figure 21 the conductivity data lines are overlain onto the regolith map of the area. Again there seems to be nothing within the data that suggest that there is a consistent correlation with aspects of the landscape and the conductivity response, apart from the springs.

Fractal Dimension and Regolith

In Figure 22 the fractal dimension data lines are overlain onto the regolith map of the area. As with the conductivity, there appears to be no direct correlation between the fractal dimension and the regolith. There is some correlation between the signatures of the springs; however this is not consistent over the whole of the survey area. The alluvial channels and depressions have no consistent value, while some areas that were known to be saturated have high fractal dimension, whilst others, again saturated, are low.

Discussion

Conductivity of the Mound Springs

Patterns in the conductivity response from the survey area at Wabma Kadarbu had varying degrees of correlation to observed changes in the regolith and landscape, as a whole this was not as much as was expected. These aspects of the responses are illustrated in Figure 20, as well as the annotated images shown in Figure 22.

One feature of the landscape with which there is correlation with the conductivity response is the mound springs. The springs, both extinct and active, produce a low conductivity signature, usually below 100 mS/m. The low conductivity signature of the extinct springs can be explained through the carbonates that make up the 'mound' structure of the spring (Figure 22f, h). For the active springs (Figure 22a, e, i k,) the carbonate composition is also a factor, however there is also the added contribution of the relatively fresh water that is discharged out of the springs, which had measurements between 6.57- 5.22 mS/cm (Table 1).

The discharge area from The Bubbler produces a higher overall conductive signature, however there are some areas with a lower conductivity. These areas can be explained by the carbonates that are present in this area, as a result of a build of the precipitates discharged from The Bubbler (Habermehl 1980; Keppel 2011). The water that flows, collects and evaporates from here has a more concentrated amount of dissolved solids and salts, and as such the conductivity is higher.

Another feature of the conductivity response that was relatively consistent is a higher conductivity with alluvial regolith land form units. This does not hold true for all areas classified as an alluvial landform, but in many areas, (Figure 22b,g) it is the case. This could be due to an observed increase of moisture within some of those areas (Figure 22m, g) which may be the result of recent rainfall that has subsequently pooled in those drainage depressions. However the elevation in this

area is not noticeably lower than other places in the survey area, thus this does not provide a simple explanation for the conductivity difference (Figure 11).

Some of the regions that are relatively conductive in the survey area relate to areas where sticky grey green clay was found in the shallow subsurface. These clay rich zones could be smectitic (Munday 2009). The presence of smectite is liable to result in a higher conductivity, as they are sheet silicates and will readily take water in between these layers (Eggleton 2001). The water is bound as molecules to exchangeable Ca, K, Mg, or Na, and smectites typically form the finest particles within the soil (Eggleton 2001). Having observed this in some areas, it is possible that the areas that are conductive but appeared to be sandy may have a thicker layer of this clay immediately below the surface.

The water when first discharged from the spring is relatively fresh, shown by the distinctive low conductivity areas, however due to the age of the springs and the amount of dissolved solids that are being brought up from the subsurface (Herczeg *et al.* 1991) the concentration of salts in the area has an effect on the conductivity. The major springs in the survey area, Blanche Cup and The Bubbler have been dated at 15.1 $\pm$ 2.2 ka and 10.9 $\pm$ 1.5 ka, respectively (Prescott & Habermehl 2008). Thus this considerable period of time may be a contributing factor to the high saline content of the area, which causes incongruity within the conductivity responses (Munday 2009).

The high salt precipitation may also be due to the contact of GAB aquifers with older, more saline, Permo-Triassic rocks in the south west of the basin, increasing the salinity of the groundwater relative to the other parts of the GAB (Habermehl 1980; Cox 1998). The concentration of dissolved solids within the south western part of the GAB may also be attributed to the dissolution of evaporates, carbonate minerals or clay minerals (Herczeg *et al.* 1991).

Thus there are a number of ways in which the conductivity response reflects aspects of the landscape. However, there is also much of the data which has no apparent correlation to the landscape. There are also areas that do not seem to have direct correlation to a water source within

the landscape despite their high conductive response (Figure 23c, d, l). In part this lack of relationships and correlation is related to the volume averaging nature of EM methods. The use of spatial based power spectra and fractal analysis will further asses the variation in the landscape, and the correlation between the conductivity and the landscape.

In-phase and conductivity relationship:

The measured in-phase signal component is an indication of magnetic susceptibility commonly used for identifying anthropogenic materials. This use is effectively demonstrated by the highs observed at the fences around the two major springs, The Bubbler and Blanche Cup (Figure 13). It is observed that the in-phase followed the trends of the conductivity, although with less high frequency variance (Figure 23). This lack of variation is more apparent on the mapped plots, as the majority of the data points are in the lower regions of the scale, below -30 000 ppt (Figure 13). It is interesting to note that although areas of high measurement are the same between the two different plots, the areas that had more significant highs in the conductivity are not observed in the in-phase measurements. This can be seen in Figure 13, where the area within The Bubbler tail is much higher than the other lines, and also more apparent than the high as it appears in the conductivity map. The major area of high conductivity within the conductivity data, between the two extinct springs along Grid Line D, is not as a whole as high within the in-phase data. There are a few areas which remain high points within the in-phase data, which were not as significant within the conductivity data, these being the small high point in about the middle of Grid Line C, while the two areas along Grid Lines F and G are significant in the conductivity and retain some of that characteristic within the in-phase data.

The variation between in-phase components and conductivity highlight the competing influences of mineralogy, water content and salinity. Unlike the conductivity the in-phase component is not affected by water or salinity.

Fractal dimension and conductivity:

The observed response of the fractal dimension is, in a number of respects, not consistent with the findings from the regolith map and the conductivity response. The fractal dimension of the springs is not consistent (Figure 21) with values varying from low to high in these areas.

There does seem to be some consistency with the comparison between the areas that had unexplained high conductivities as already mentioned. In all of these areas the fractal dimension remains quite low (Figure 21).

There are some relationships between the fractal dimension and the conductivity, which can be seen in the three areas (a-c) highlighted in Figure 24 and 25. These areas show differing and consistent contrasts between the fractal dimension and the conductivity. The first area that has been highlighted, labelled as zone a) shows an area of high conductivity, consistent along both the G and H grid lines, with high on conductivity at the edge of an alluvial landform followed by an area of mid range conductivity at the transition to The Bubbler runoff. This correlates with an area of low and then high fractal dimension. As said before it is thought that a higher fractal dimension correlates with longer wavelengths and thus deeper features in the subsurface as well as a more heterogeneous earth. While the lower fractal dimension values correlate with a homogenous earth, shorter wavelengths and thus shallow features in the subsurface as well as random noise. Taking this into consideration, it could be said that a) shows an area where the subsurface moves from homogenous to heterogeneous, perhaps reflecting some subsurface structure.

The zone labelled b) is an area of correlating high conductivity across two lines, which has resulted in a low fractal dimension. In terms of the regolith, the boundary between two regolith landform units is east-west while the correlation is north-south. This could be an indication of a homogeneous earth at a shallow depth, and the fractal dimension correlation between the two areas across the different regolith units could indicate the lack of effect that the regolith has on the fractal dimension.

The zone labelled c), which is situated towards the south western end of Line C has the same correlation pattern as previously highlighted in a), with the high conductivity relating to a low fractal dimension. What is interesting in this area is that the low fractal dimension is flanked by two areas of high fractal dimension. This correlates to what is seen with the conductivity, with the high flanked by low conductive responses. This response is also highlighted in Figure 26c, as the low in conductivity corresponds to a high within the conductivity. Thus there is an inverse correlation that can be seen within the fractal dimension. This area is also on the boundary between regolith units, where the CHpp unit moves to the CHer unit, at the base of Hamilton Hill, the elevation of the area also changes (Figure 11). Thus the fractal dimension here may be giving an indication of a change in the underlying geology, shown by the move into the CHer unit on the surface.

The areas illustrated in Figure 26 demonstrate how the fractal dimension and the conductivity can correlate, and how it can also show no correlation. Points a) and d) show an inverse correlation between the conductivity and the fractal dimension, with the two low areas of conductivity showing high areas of fractal dimension. However points b) and c) illustrate how the fractal dimension and conductivity do not correlate in some areas. The highest spike in conductivity is seen at point c), which contains a number of fractal dimension points not showing any correlated decrease, which could have been expected. Point b) is different again, as instead of showing an inverse- or no- correlation it has a direct correlation between a low in the conductivity and a low in the fractal dimension.

These datasets show examples of how it is extremely difficult to characterise the fractal dimension of an area, especially in relation to conductivity and the regolith. There are some relationships between the different datasets however at this point what exactly those relationships are is difficult to ascertain at this time, without further field investigation. Due to the large amount of variation that was found within the survey area and datasets, the aim to characterise and better understand the movement of groundwater and fluid flow in the subsurface was not achieved as well

as hoped at the outset. The influence of saline groundwater, concentrated precipitates and the general complexity of the soil composition in the survey area resulted in data that was difficult to characterise with any degree of confidence. However there are some correlations which may, with further study, be able to reveal more in regards to modelling fluid flow and groundwater movement.

For further study, one aspect that would be interesting to look at would be the comparison of the fractal dimension of the smaller, local dataset, with a fractal dimension of a larger, regional dataset. This could be achieved by looking at the Frome AEM data, which was collected by Geoscience Australia in 2010. Due to time constraints this was deemed to be beyond the scope of this project, however a fractal dimension filter, such as a variation filter, or a wavelet transform could provide quite interesting results (Dhu *et al.* 1999; Dhu *et al.* 2000; Kirby & Swain 2004). These larger scale datasets allow for a longer wavelength to be able to get information out of the dataset, providing a greater bandwidth. This could then provide a comparison as to whether or the fractal dimension is a useful filter for the regional scale data, which Dhu (2008; 2010) suggests it is, as compared to the information that we were able to gain from it on a local scale.

Further investigation could also examine the use of different window sizes. It may be that part of the problem is that the 64 point moving window did not allow for enough low frequency data while a 128 point window would allow for this. It would also be interesting to compare the power spectra that was calculated for the fractal dimension, i.e. for every point, to that which would be produced by an FFT of the whole line, such as produced by Everett and Weiss (2002).

Conclusion

From the data collected at Wabma Kardabu National Park, it can be concluded that the mound springs have a strong resistive signature with a conductivity survey. Due to the saturation from groundwater and concentration of the discharged salt and solids from this groundwater, much of the remaining survey area does not exhibit a consistent conductive signature. This makes it hard to quantify what relationship, if any, exists between these different aspects. It was hoped that by using fractal dimension as an extra means of processing conductivity data it would reveal further information regarding the subsurface.

Further studies could look into the use of different filters and transforms and different sized sample areas. There are a number of different methods of achieving this, through the wavelet and fractal dimension variation filters.

Recent, higher than average, rainfall in the area may have provided some of the high conductivity in the area. Thus it would interesting, in terms of the results of the conductivity survey, to the temporal and climatic effects in the area when the rainfall had been closer the average amount that area would normally receive.

A more thorough analysis of the soil content and percentages of clays and sands, as well as the salt content would also be an area for further research. This could possibly reveal further information as to the relationship between the conductivity and the regolith which was missed during the less detailed study conducted through the course of this project.

Further investigation into fractal dimension signatures could also be done by conducting similar sized surveys, but in areas of known and contrasting lithologies. It would be expected that these surveys would be able to be compared and contrasted to a greater degree and with more of a viable outcome than just the comparison of the conductivity and fractal dimension revealed in this study.

In regards to the original aims; to better understand the flow mechanisms that control the mound springs, this not been able to be achieved within the scope of this study. The large amount of variation within the conductivity response, and the subsequent variation within the fractal dimension, did not allow for any definite conclusions as to fluid pathways or movement within the subsurface of the survey area. Further study into looking at larger data sets may be able to better characterise fluid flow and groundwater movement with the subsurface.

Acknowledgements

I would like to thank Graham Heinson for his continued support throughout the year.

Many thanks go to Mike Hatch, Kent Invarity, Justin Payne and Katie Howard for their invaluable time and assistance with many and varied aspects of this thesis, including data processing, editing and explaining concepts several thousand times.

My thanks also go to this year's Honours group – without whose support, advice and mutual ranting this year would have been quite different. To Room G110, the hours spent within that office were made bearable by the people who I shared it with.

To my fellow gee-whizzical kids, thanks for making fieldwork, coursework and MTEC events to remember, as well as your support throughout the year.

To my friends outside of G&G, my thanks go for listening to many one sided (and terribly boring) conversations regarding my thesis, and their understanding with my absence from various social events and their lives in general for the past three months.

And to my long suffering family, most especially my darling mum and brother, thank you for understanding how important this year was and for being an invaluable support, without which I couldn't have achieved half so much as I did.

References

ADLER P. M. & THOVERT J. F. 1993. Fractal porous-media. *Transport in Porous Media* **13**, 41-78.

ALDAM R. K., K.S. 1988. *An Investigation of the Structures Controlling Discharge of Spring Waters in the South Western Great Artesian Basin* Department of Mines and Energy S. A.**:** 1-16. DME, Adelaide

ANDRLE R. 1992. Estimating fractal dimension with the divider method in geomorphology. *Geomorphology* **5**, 131-141.

BERRY M. V. & LEWIS Z. V. 1980. On the Weierstass-Mandelbrot fractal function. *Proceedings of the Royal Society of London Series a-Mathematical Physical and Engineering Sciences* **370**, 459-484.

BURGER H. R., SHEEHAN, A.F., JONES, G.H. 2006. *Introduction to applied geophysics:exploring the shallow surface* (Revised Edition edition). W. W. Norton & Company

CARR J. R. 1997. Statistical self-affinity, fractal dimension, and geologic interpretation. *Engineering Geology* **48**, 269-282.

CARR J. R. & BENZER W. B. 1991. On the practice of estimating fractal dimension. *Mathematical Geology* **23**, 945-958.

CHILÈS J. 1988. Fractal and geostatistical methods for modeling of a fracture network. *Mathematical Geology* **20**, 631-654.

COX R. A. B., A. 1998. Great Artesian Basin: Resource Study. *The Great Artesian Basin Consultative Council*.

DHU T. 2008. The use of fractal dimension for texture-based enhancement of aeromagnetic data. Thesis (Ph.D.) thesis, Australian School of Petroleum, University of Adelaide Adelaide (unpubl.).

DHU T., DENTITH M. C. & HILLIS R. R. 1999. The use of fractal dimension estimators for enhancing airborne magnetic data. *Exploration Geophysics Melbourne* **30**, 1-2.

DHU T., DENTITH M. C. & HILLIS R. R. 2000. Enhancement of airborne magnetic data using the variation method of fractal dimension estimation. *Preview* **84**.

DHU T. & HEINSON G. 2010. Fractal scaling of airborne EM data; an indicator of lithology and fluid connection? *Australian Society of Exploration Geophysicists Perth, West. Aust., Australia. Pages* **1**.

DHU T., HEINSON G. & JOSEPH J. 2004a. The hydraulic and electrical fractal dimension of regolith. *Australian Society of Exploration Geophysicists Perth, West. Aust., Australia., Petroleum Exploration Society of Australia Sydney, N.S.W.*

DHU T., HEINSON G. & JOSEPH J. 2004b. Viewing the regolith through different eyes: a new way of interpreting resistivity data. *Cooperative Research Centre for Landscape Environments and Mineral Exploration Bentley, West. Aust., Australia. Pages*.

DHU T., HEINSON G. S. & JOSEPH J. 2003. The hydraulic and electrical fractal dimension of regolith. *Cooperative Research Centre for Landscape Environments and Mineral Exploration Bentley, West. Aust., Australia. Pages*.

EGGLETON R. A. (Editor) 2001. *The Regolith Glossary*. CRC LEME, Canberra

EVERETT M. E. & WEISS C. J. 2002. Geological noise in near-surface electromagnetic induction data. *Geophysical Research Letters* **29**.

FARDIN N., STEPHANSSON O. & JING L. R. 2001. The scale dependence of rock joint surface roughness. *International Journal of Rock Mechanics and Mining Sciences* **38**, 659-669.

FENSHAM R., J. AND FAIRFAX, R.J. 2003. Spring wetlands of the Great Artesian Basin, Queensland, Australia. *Wetlands, Ecology and Management* **11**, 343-362.

FOX C. G. 1989. Empirically derived relationships between fractal dimension and power law form frequency-spectra. *Pure and Applied Geophysics* **131**, 211-239.

G.F. INSTRUMENTS *Short Guide for Electromagnetic Conductivity Survey*. GF Instruments, Czech Republic

GF INSTRUMENTS *Short Guide for Electromagnetic Conductivity Survey*. GF Instruments, Czech Republic

HABERMEHL M. A. 1980. The Great Artesian Basin, Australia. *BMR Journal of Australian Geology and Geophysics* **5**, 9-38.

HABERMEHL M. A. 1982. *Springs in the Great Artesian Basin, Australia - Their Origin and Nature*. Energy D. o. N. D. a. Australian Government Publishing Service

HABERMEHL M. A. 2001. Hydrogeology and environmental geology of the Great Artesian Basin, Australia. *Special Publication Geological Society of Australia* **21**, 127-143.

HARRIS C., LEWIS, S., ANGAS, H. 1997. *South Australia's Mound Springs: Maintenance and Imporovement of their Environement and Heritage Values*. Department for Environment and Heritage S. A., Australia 1-11, Adelaide

HERCZEG A. L., TORGERSEN T., CHIVAS A. R. & HABERMEHL M. A. 1991. Geochemistry of ground waters from the Great Artesian Basin, Australia. *Journal of Hydrology* **126**, 225-245.

HOWARD R. M. 2003. *Principles of Random Signal Analysis and Low Noise Design: The Power Spectral Density and its Applications*. John Wiley & Sons, Inc, New York

KEAREY P. 2001. *Dictionary of Geology*. *Dictionary of Geology***:** 327. Penguin, London.

KEPPEL M. N., CLARKE, J., HALIHAN, T., LOVE, A., WERNER, A. 2011. Mound springs in the arid Lake Eyre South region of South Australia: A new depositional tufa model and its controls. *Sedimentary Geology*, 16.

KIRBY J. F. & SWAIN C. J. 2004. Global and local isostatic coherence from the wavelet transform. *Geophysical Research Letters* **31**.

KRIEG G. W., ROGER, P.A., CALLEN, R.A., BELPERIO, A.P. AND FORBES, B.G. 1992. *CURDIMURKA map sheet*. South Australia, Geological Survey.

LOVE A. A. K., M. 2008. Desktop review of potential groundwater interconnectivity between Ackaringa and Great Artesian Basins *Coffey Environments*

MANDELBROT B. B. 1977. *The Fractal Geometry of Nature* (2nd Edition edition). W. H. Freeman and Company New York

MANDELBROT B. B. 1985. Self-affine fractals and fractal dimension. *Physica Scripta* **32**, 257-260.

MCNEILL J. D. 1980. Electromagnetic Terrian conductivity Measurement at Low Induction Numbers *Geonics Ltd.* .

MCNEILL J. D. 1991. Advances in electromagnetic methods for groundwater studies. *Geoexploration* **27**, 65-80.

MUDD G. M. 2000. Mound Springs of the Great Artesian Basin in South Australia: a case study from Olympic Dam. *Environmental Geology* **39**, 463-476.

MUNDAY T. 2009. Regolith Geophysics *In:* Scott K. M. a. P., C.F. ed., *Regolith Science* pp 219-250, CSIRO.

PRESCOTT J. R. & HABERMEHL M. A. 2008. Luminescence dating of spring mound deposits in the southwestern Great Artesian Basin, northern South Australia. *Australian Journal of Earth Sciences* **55**, 167-181.

PRESS W. H., ET. AL. 1992. *Power Spectrum Estimation Using the FFT N, sec. 13.4, Numerical Recipes in C* (2nd ed. edition). Cambridge University Press.

RADKE B. M., FERGUSON, J., CRESSWELL R.G., RANSLEY, T.R., HABERMEHL, M.A., 2000. *Hydrochemistry and implied hydrodynamics of the Cadna-owie-Hooray Aquifer, Great Artesian Basin*. Department of Agriculture F. a. F., Australia**:** 229. Bureau of Rural Sciences Canberra

RENSHAW C. E. 1998. Sample bias and the scaling of hydraulic conductivity in fractured rock. *Geophysical Research Letters* **25**, 121-124.

THEILER J. 1990. Estimating fractal dimension. *Journal of the Optical Society of America a-Optics Image Science and Vision* **7**, 1055-1073.

TURCOTTE D. L. 1989. Fractals in geology and geophysics. *Pure and Applied Geophysics* **131**, 171-196.

TURCOTTE D. L. 1997. *Fractals and Choas in Geology and Geophysics* (2nd Edition edition). Cambridge University Press Cambridge

TYLER M. J., TWIDALE, C.R., DAVIES, M. AND WELLS, C.B. (Editor) 1990. *Natural History of the North East Deserts*. The Royal Society of South Australia In. , Adelaide.

WEISSTEIN E. W. 2011. "Power Spectrum." <http://mathworld.wolfram.com/PowerSpectrum.html >. (retrieved 1-10-2011 2011).

WELSH W. D. 2006. *Great Artesian Basin: transient groundwater model*. Sciences B. o. R., Canberra.

WILLIAMS A. F. & HOLMES J. W. 1978. Novel method of estimating discharge of water from mound springs of Great Artesian Basin, Central Australia *Journal of Hydrology* **38**, 263-272.

Tables:

Table 1: Table showing the resistivity and conductivity of the spring's discharge. These were sampled both at the survey area, and at other springs with the Lake Eyre spring group.

				Estimate from TDS	Measurements standardised to 25 degrees C				
Cobb 1975 Report Book 75/90	EC (uS/cm) -- units triple checked	TDS (mg/L)	Disch -arge (L/s)	EC (mS/cm)	uS/cm	mS/cm	S/cm	S/m	ohm.m
The Bubbler	5600 at 24 deg		7.5		5330	5.33	0.00533	0.533	1.88
Blanche Cup	5900 at 14 deg				5650	5.65	0.00565	0.565	1.77
Blanche Cup	7000 at 28 deg				5958	5.958	0.005958	0.5958	1.68
"Spring 5" = Little Bubbler	5600 at 24 deg				5050	5.05	0.00505	0.505	1.98
Beresford	6600 at 22 deg				5550	5.55	0.00555	0.555	1.80
Warburton	6600 at 24 deg				6640	6.64	0.00664	0.664	1.51
Kinhill Stearns report									
Beresford Railway Bore		3822		7.644		7.644	0.007644	0.7644	1.31
Coward Springs Bore		3210		6.42		6.42	0.00642	0.642	1.56
Tweed et al. 2011, J. Hydrol.									
Blanche Cup		5500		11		11	0.011	1.1	0.91
The Bubbler		4190		8.38		8.38	0.00838	0.838	1.19
Adelaide uni samples tested 9/8/11									
The Bubbler						5.32	0.00532	0.532	1.88

Warburton Spring						6.22	0.00622	0.622	1.61
Beresford Spring						8.85	0.00885	0.885	1.13
Strangways Spring south						8.34	0.00834	0.834	1.20
Strangways Spring north						6.1	0.0061	0.61	1.64
Little Bubbler						4.68	0.00468	0.468	2.14
Blanche Cup						6.85	0.00685	0.685	1.46
Adelaide uni samples tested 9/11/11									
Main creek on Wabma access road						28.3	0.0283	2.83	0.35
Warburton Spring						6.57	0.00657	0.657	1.52
Little Bubbler						5.22	0.00522	0.522	1.92

Figure Captions:

Figure 1: Map of the Great Artesian Basin (GAB), showing the areas of recharge, situated towards the eastern margins of the basin, in grey. The extent of the GAB itself is highlighted in blue, with major spring groups and the direction of groundwater flow also highlighted. The survey area was situated within the Lake Eyre Spring group, highlighted by the red box. The image is after Fensham (2003).

Figure 2: Cross section of the GAB, after Radke (2000). Cross section of the GAB from East-West, approximately across the middle of the basin. The main aquifers, including the Cadna-owie- Hooray, are highlighted in blue. This is the aquifer which is of most importance to the survey area. The confining beds are shaded in grey, with the main confining bed that is of interest to our survey is the Bulldog Shale.

Figure 3: General cross section of a mound spring. The diagram shows how the confining beds concentrate the water flow, and the influence of local faulting to the discharge of the spring. The

build up of precipitates, and the pooling of water after discharge, forming swamps and areas of saturation. This is a broad idea of what is thought to be the structure of the springs in the survey area. This image is after Mudd (2000).

Figure 4: Map showing the major springs within the Lake Eyre Group. These include The Bubbler and Blanche Cup, highlighted again in red. Image after Harris (1997).

Figure 5: Showing the electromagnetic survey instrument, CMD-4 in use, in the survey area**.**

Figure 6: High resolution map, georeferenced Google Earth Images, with the survery lines and major features. The coloured lines are the three tie lines, A, B and C. The Grid lines are shown in black, the assignation of labels occurring from the south to north, A, B, C... H. The prominent mound springs in the survey area are also labelled, The Bubbler, Blanche Cup and Hamilton Hill.

Figure 7: A representation of the relationship between the type of the earth, the EM signature that it generates and the power spectra that is the result. A homogenous earth theoretically results in an even EM signature, which then correlates to a nil slope of the power spectrum. This in turn results in a low fractal dimension value. A heterogeneous earth, populated with faults and fractures for example, results in an EM signature with an increase in high frequency variability; this in turn creates a slope of the power spectrum and an increase in the fractal dimension value.

Figure 8: An example of the re-sampling of the conductivity. Points were re-sampled to give a value of the conductivity every two meters. This allowed for the power spectra slopes to be produced through FFT, and the fractal dimension to be calculated.

Figure 9: Examples of the output of the data processing. a) The slopes of the power spectrum, which were calculated for each point; b) The fractal dimension, due to the calculation not being a linear function error bars are part of the output of the data, while the black line represents a moving average of the point and allows for a discrete value of the fractal dimension to be calculated; c) The re-sampled conductivity graph allows for comparison between different data sets.

Figure 10: Conductivity data lines plotted using GIS software allow for the changes in conductivity over the landscape and landscape features to be seen.

Figure 11: The elevation of the data points, taken whilst using the differential GPS, have been plotted on the same map as the conductivity. This allows for comparison between the two data sets and any correlations can be seen. The elevation is plotted at a smaller sized data point and 20m to the north of the conductivity to allow for comparison.

Figure 12: Contour map for the conductivity. The points plotted here have not been re-sampled.

Figure 13: In-phase data lines plotted using GIS software allow for the changes in conductivity over the landscape and landscape features to be seen.

Figure 14: Fractal dimension data lines plotted using GIS software allow for the changes in conductivity over the landscape and landscape features to be seen.

Figure 15: Contour map of the fractal dimension. This example is modelled at 5m data intervals.

Figure 16: Regolith-landform map of the survey area. Classifications were made from aerial photo interpretation and field observations.

Figure 17: Unit descriptions used in the regolith landform map.

Figure 18: Example of the graph plotting the re-sampled conductivity and the fractal dimension against one another. This allowed for comparison between the fractal dimension and the conductivity.

Figure 19: The fractal dimensions and the conductivity have been plotted on the same map as the conductivity. This allows for comparison between the two data sets and any correlations can be seen. The fractal dimension lines are plotted 20m to the north of the conductivity lines to allow for comparison.

Figure 20: Regolith map with overlaid conductivity lines. This allows for comparison between the two different datasets, and to observe any correlations between the conductivity and the regolith.

Figure 21: Regolith map with overlaid fractal dimension lines. This allows for comparison between the two different datasets, and to observe any correlations between the conductivity and the regolith.

Figure 22: Annotated map of conductivity data lines with the high resolution images. Areas of interest with a high conductivity have been marked with an oval; areas of low conductivity have been highlighted with a rectangle or square. These have been lettered to allow for comparison within the discussion.

Figure 23: Graph of the in-phase and the conductivity, showing less high frequency variation in the in-phase response compared to the conductivity.

Figure 24: Annotated map, with underlying regolith map overlaid with fractal dimension. Points a-c are further elaborated and compared with the same points in Figure 25 in the discussion.

Figure 25: Annotated map, with underlying regolith map overlaid with conductivity. Points a-c are further elaborated and compared with the same points in Figure 24 in the discussion.

Figure 26: Annotated graph of Line C, with re-sampled conductivity and fractal dimension. Points a-c illustrate the different ways in which the fractal dimension and conductivity correlate.

Figures:

Figure 1:

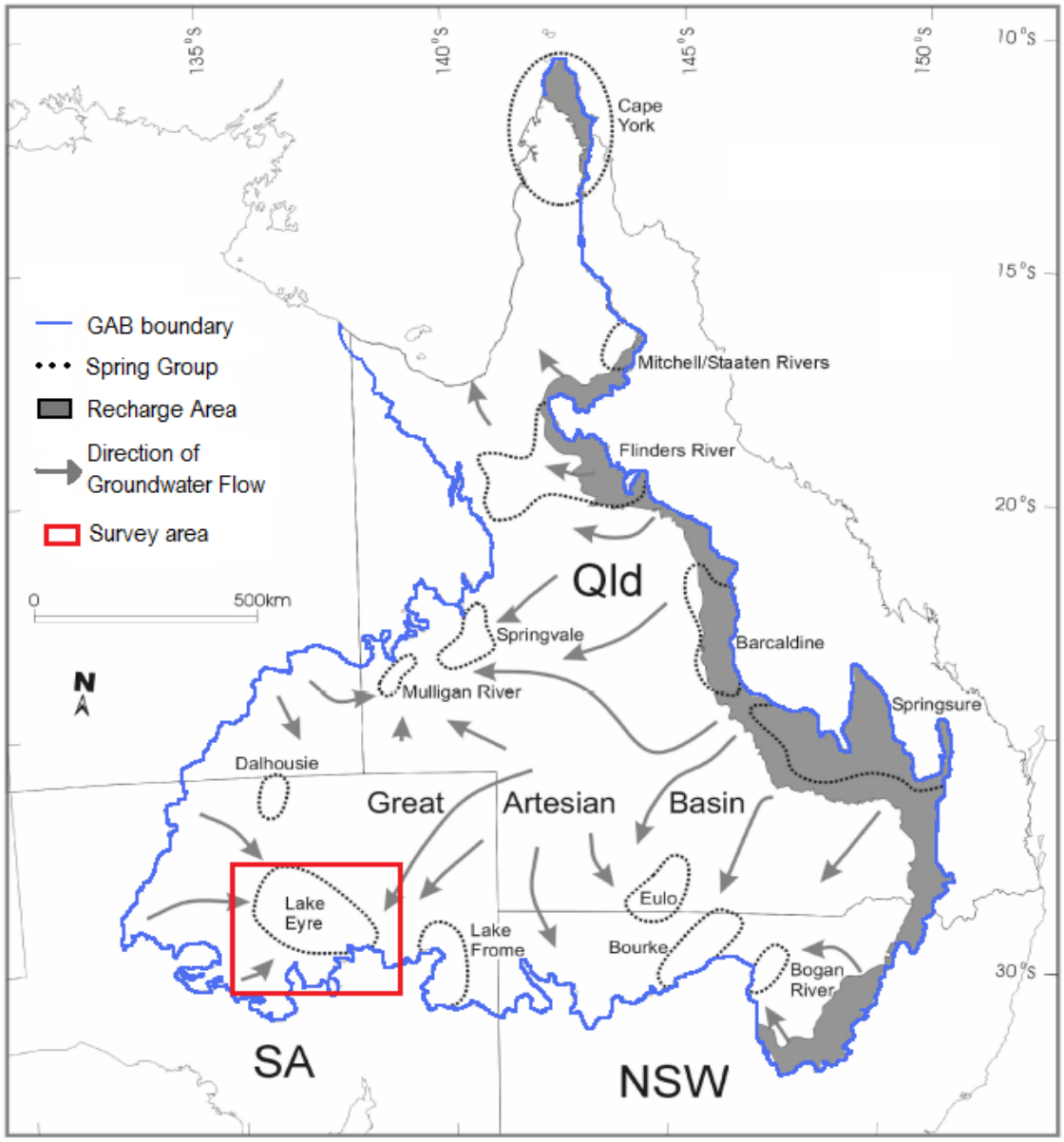

Figure 2:

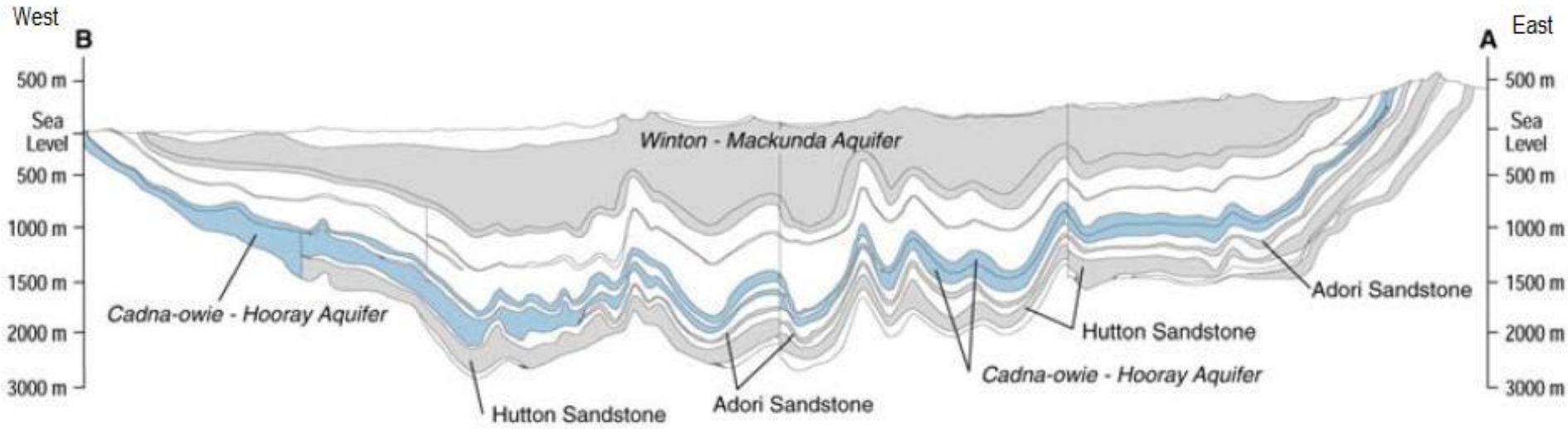
West
B
500 m
Sea Level
500 m
1000 m
1500 m
2000 m
3000 m
A
East
500 m
Sea Level
500 m
1000 m
1500 m
2000 m
3000 m
Winton - Mackunda Aquifer
Cadna-owie - Hooray Aquifer
Hutton Sandstone
Adori Sandstone
Hutton Sandstone
Cadna-owie - Hooray Aquifer
Adori Sandstone

Figure 3:

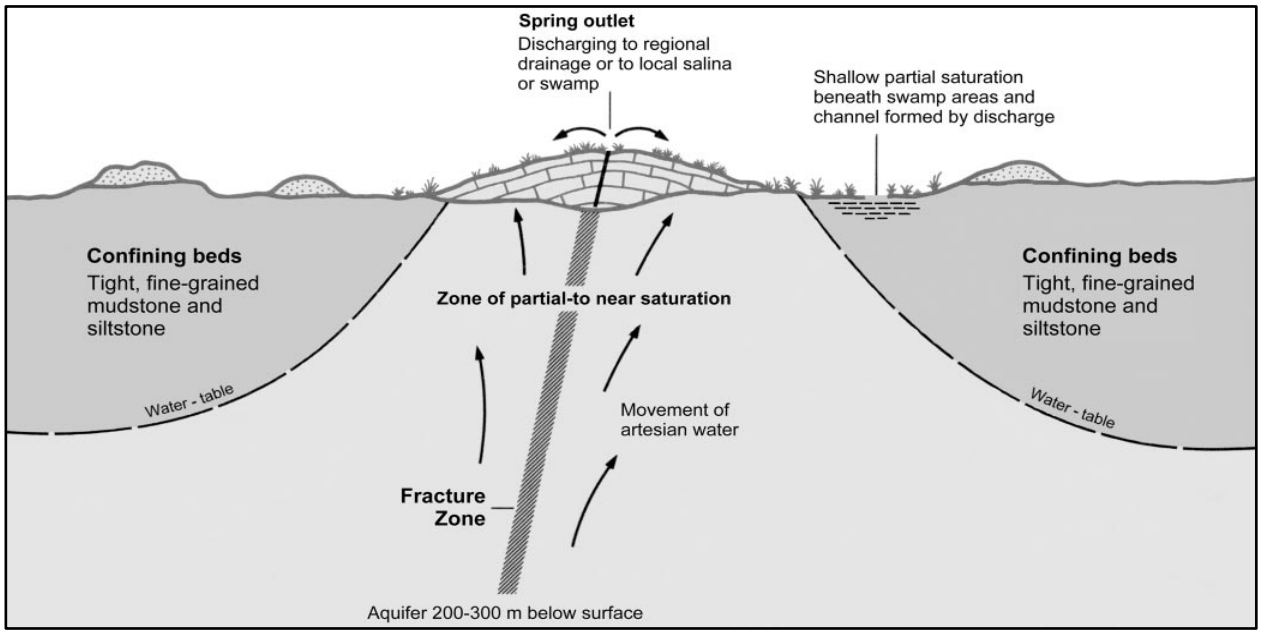
Spring outlet
Discharging to regional drainage or to local salina or swamp
Shallow partial saturation beneath swamp areas and channel formed by discharge
Confining beds
Tight, fine-grained mudstone and siltstone
Zone of partial-to near saturation
Confining beds
Tight, fine-grained mudstone and siltstone
Water - table
Movement of artesian water
Water - table
Fracture Zone
Aquifer 200-300 m below surface

Figure 4:

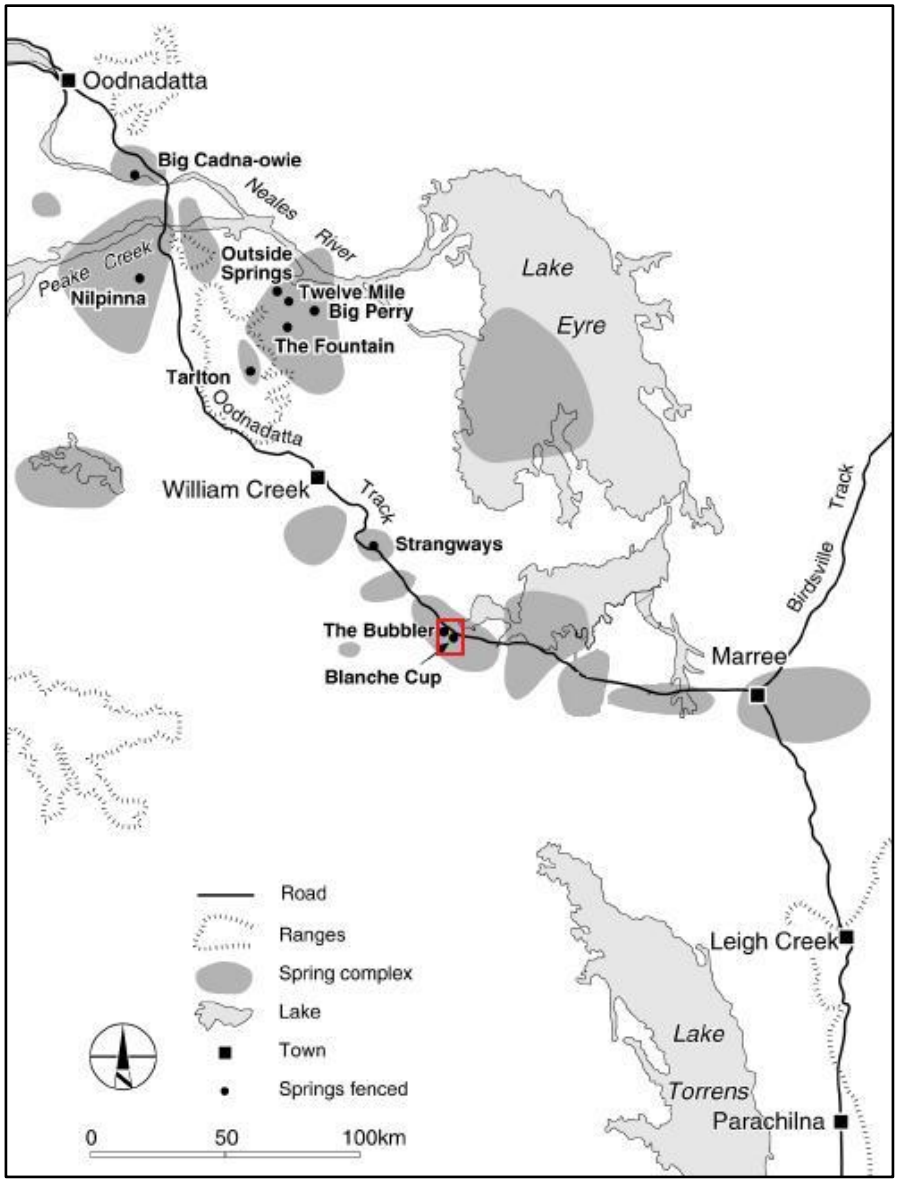
Oodnadatta
Big Cadna-owie
Neales River
Peake Creek
Nilpinna
Outside Springs
Twelve Mile
Big Perry
The Fountain
Tarlton
Oodnadatta Track
William Creek
Strangways
The Bubbler
Blanche Cup
Lake Eyre
Birdsville Track
Marree
Leigh Creek
Lake Torrens
Parachilna
Road
Ranges
Spring complex
Lake
Town
Springs fenced
0
50
100km

Figure 5:

Figure 6:

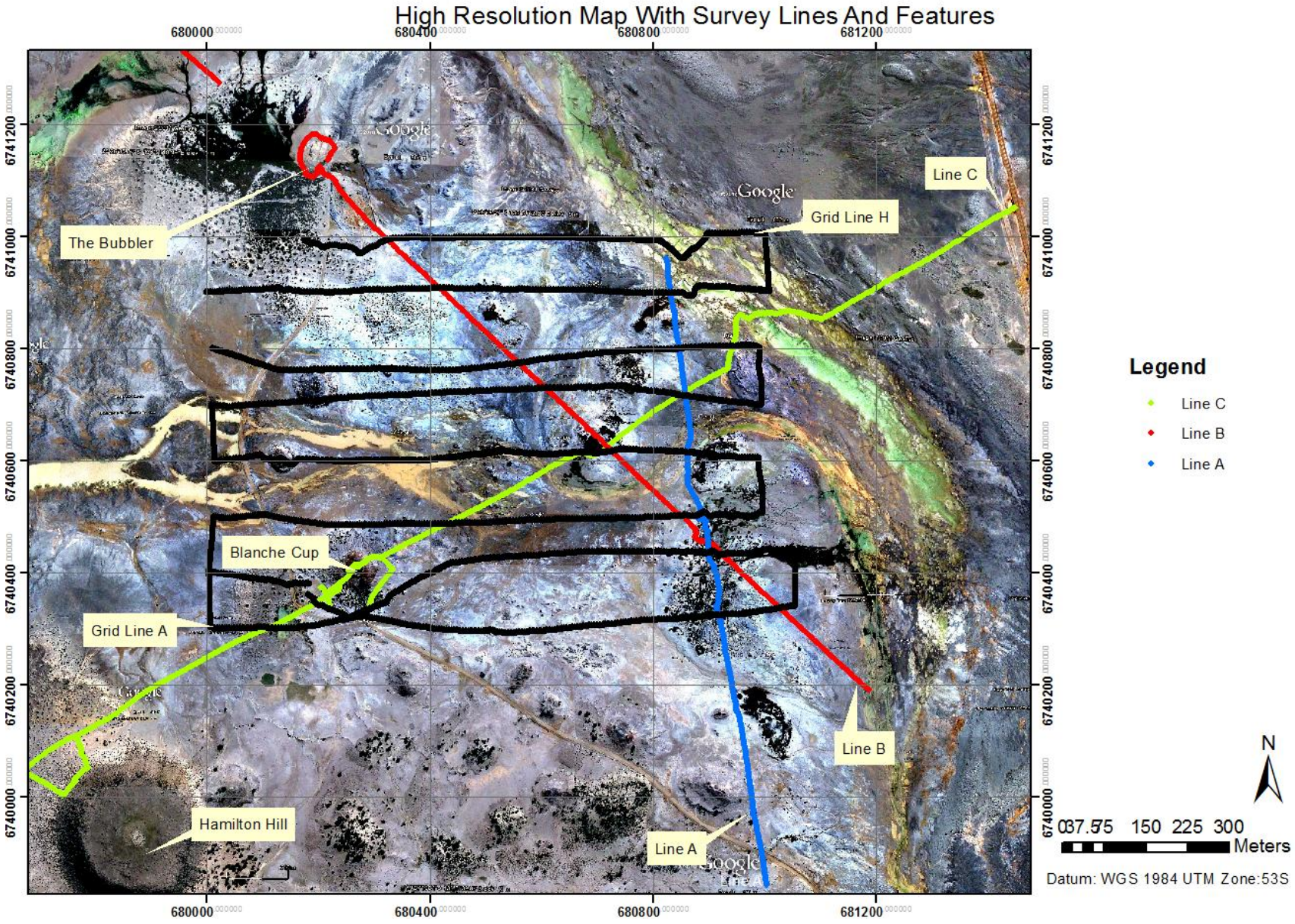
High Resolution Map With Survey Lines And Features
680000
680400
680800
681200
6741200
6741000
6740800
6740600
6740400
6740200
6740000
The Bubbler
Line C
Grid Line H
Blanche Cup
Grid Line A
Line B
Hamilton Hill
Line A
Legend
Line C
Line B
Line A
N
0 37.575 150 225 300
Meters
Datum: WGS 1984 UTM Zone:53S

Figure 7:

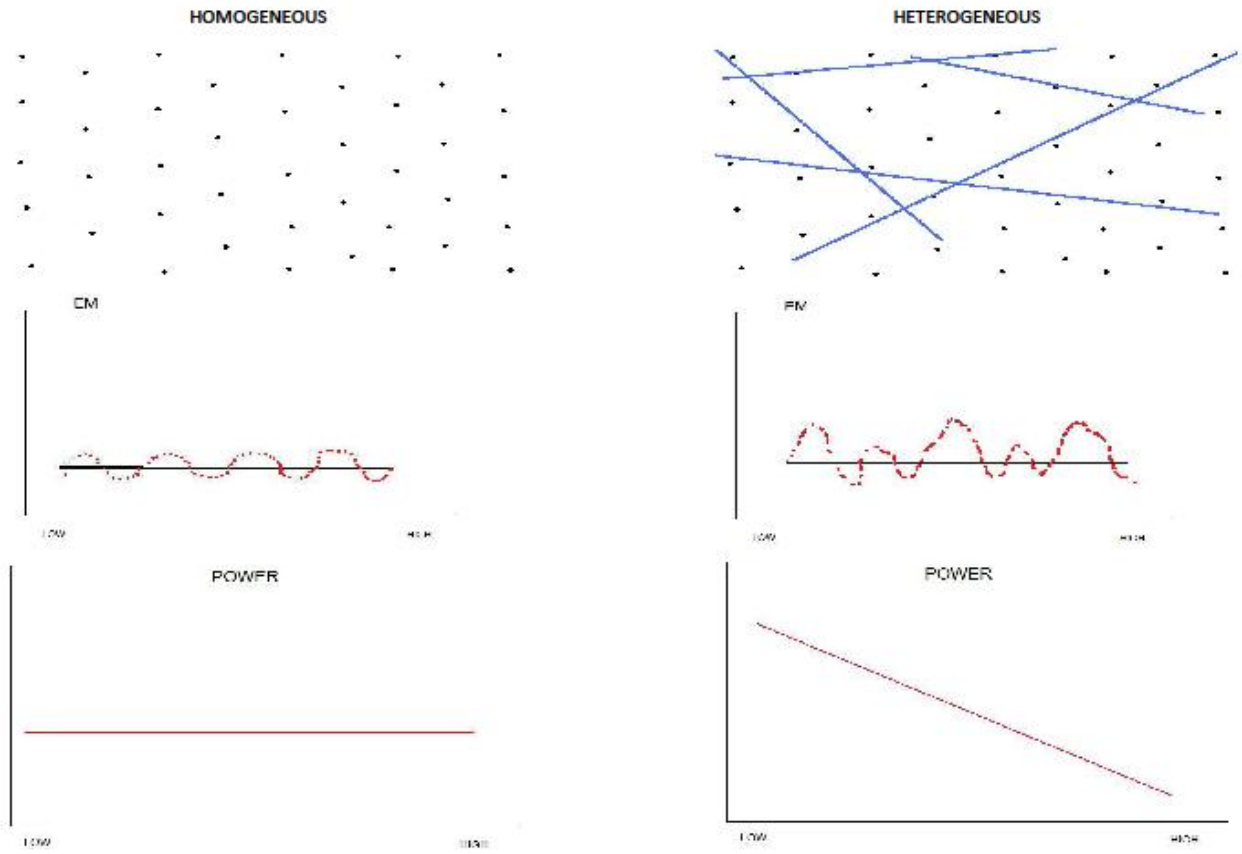

Figure 8:

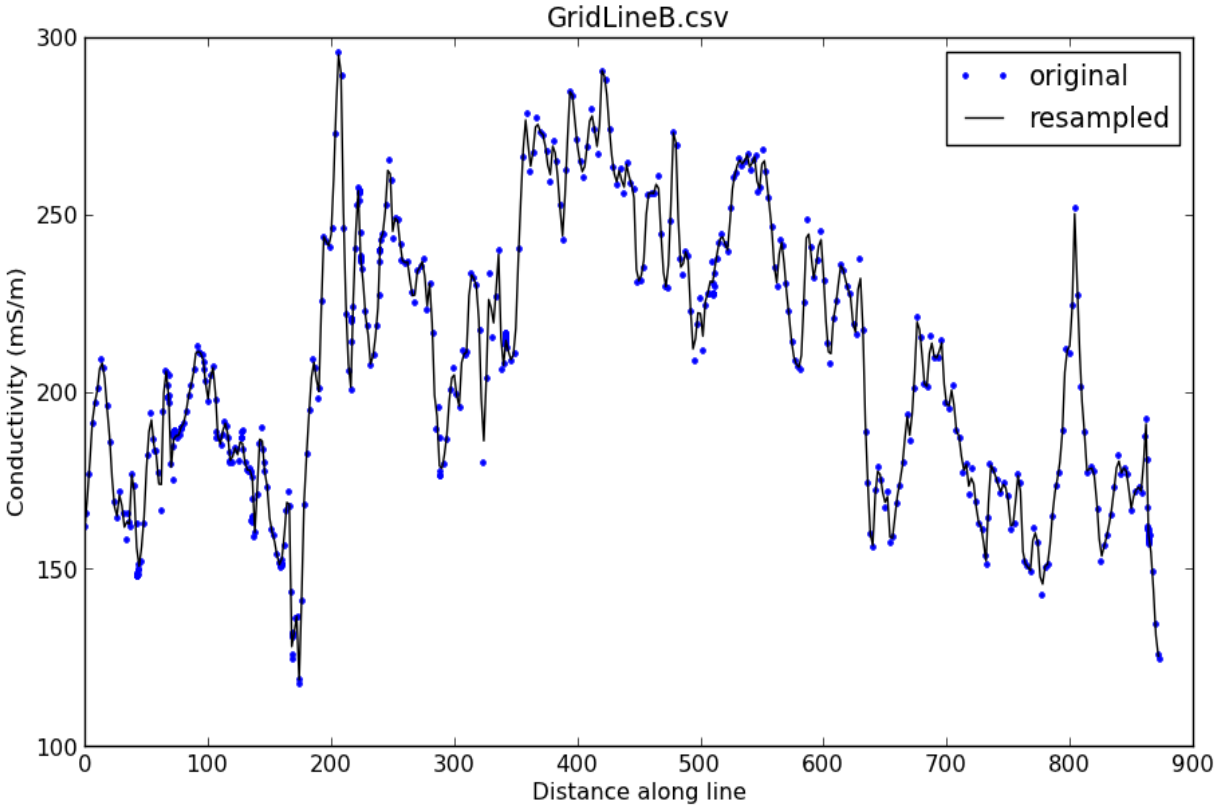
GridLineB.csv
original
resampled
Conductivity (mS/m)
Distance along line
300
250
200
150
100
0
100
200
300
400
500
600
700
800
900

Figure 9:

a.

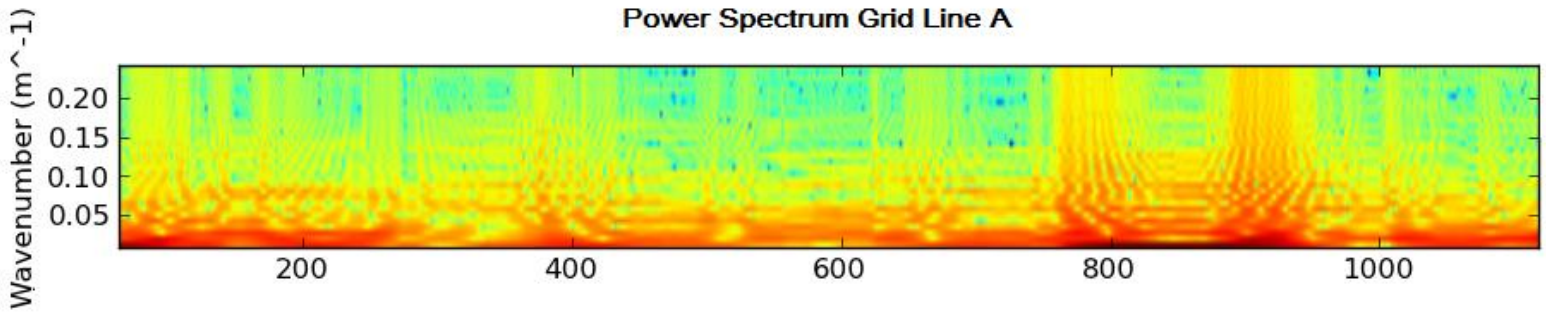
Power Spectrum Grid Line A
Wavenumber (m^-1)
0.20
0.15
0.10
0.05
200
400
600
800
1000

b.

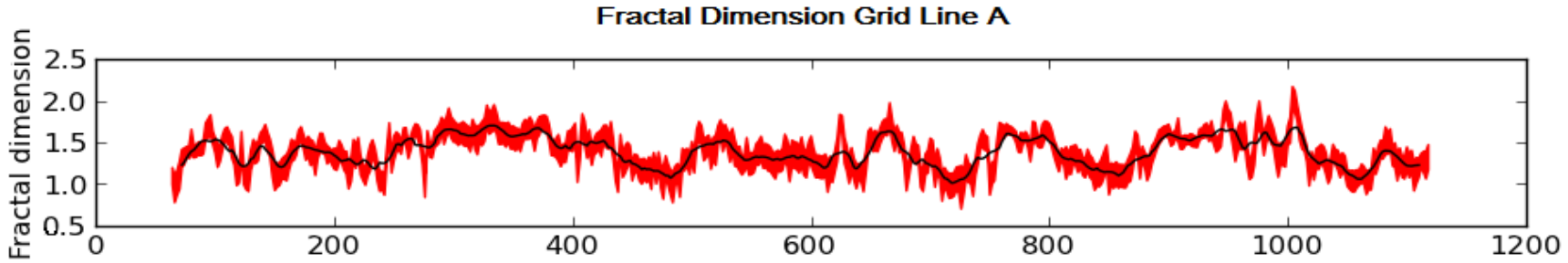
Fractal Dimension Grid Line A
Fractal dimension
2.5
2.0
1.5
1.0
0.5
0
200
400
600
800
1000
1200

c.

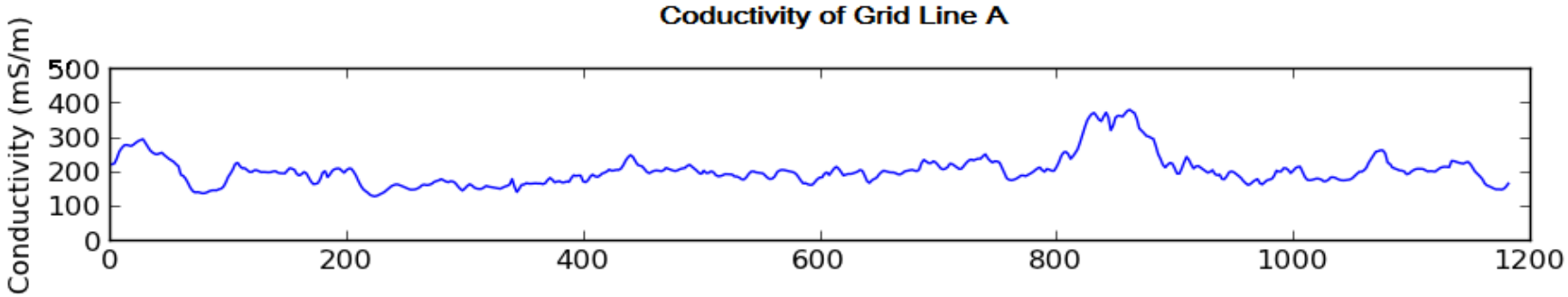
Coductivity of Grid Line A
Conductivity (mS/m)
500
400
300
200
100
0
0
200
400
600
800
1000
1200

Figure 10:

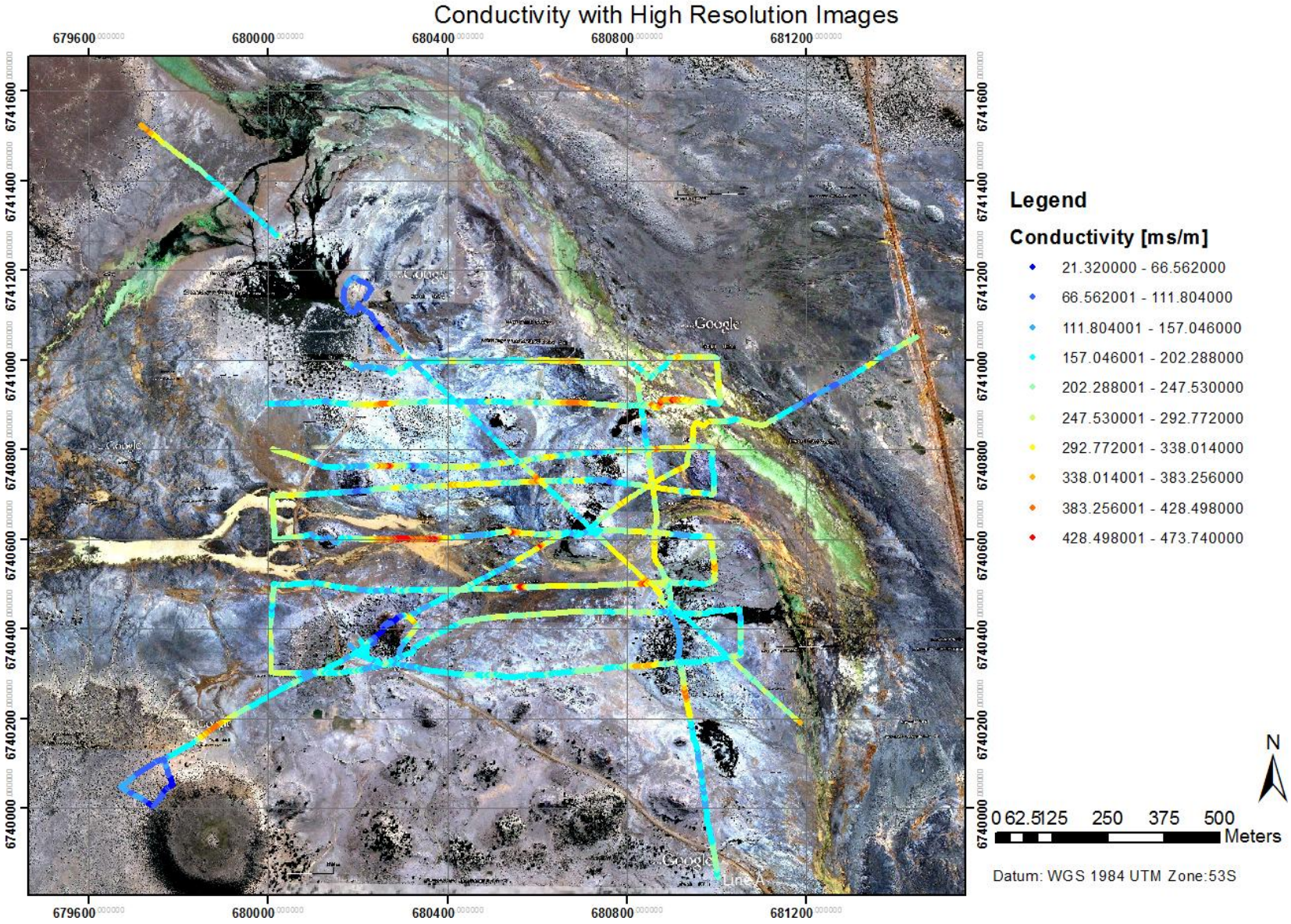
Conductivity with High Resolution Images
679600
680000
680400
680800
681200
6741600
6741400
6741200
6741000
6740800
6740600
6740400
6740200
6740000
Legend
Conductivity [ms/m]
21.320000 - 66.562000
66.562001 - 111.804000
111.804001 - 157.046000
157.046001 - 202.288000
202.288001 - 247.530000
247.530001 - 292.772000
292.772001 - 338.014000
338.014001 - 383.256000
383.256001 - 428.498000
428.498001 - 473.740000
Line A
N
0 62.5125 250 375 500
Meters
Datum: WGS 1984 UTM Zone:53S

Figure 11:

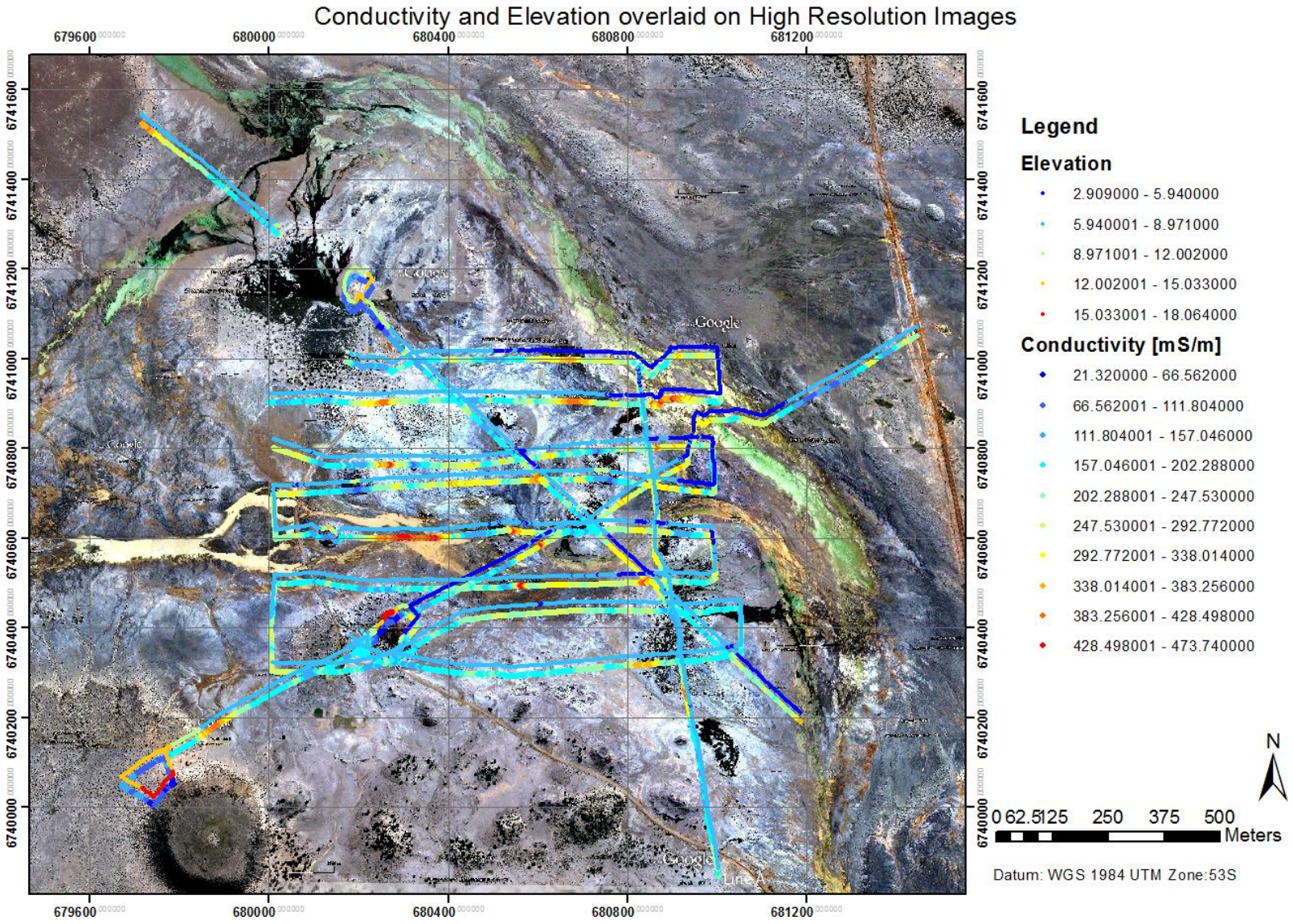
Conductivity and Elevation overlaid on High Resolution Images
679600
680000
680400
680800
681200
6741600
6741400
6741200
6741000
6740800
6740600
6740400
6740200
6740000
Legend
Elevation
2.909000 - 5.940000
5.940001 - 8.971000
8.971001 - 12.002000
12.002001 - 15.033000
15.033001 - 18.064000
Conductivity [mS/m]
21.320000 - 66.562000
66.562001 - 111.804000
111.804001 - 157.046000
157.046001 - 202.288000
202.288001 - 247.530000
247.530001 - 292.772000
292.772001 - 338.014000
338.014001 - 383.256000
383.256001 - 428.498000
428.498001 - 473.740000
N
0 62.5 125 250 375 500
Meters
Datum: WGS 1984 UTM Zone:53S

Figure 12:

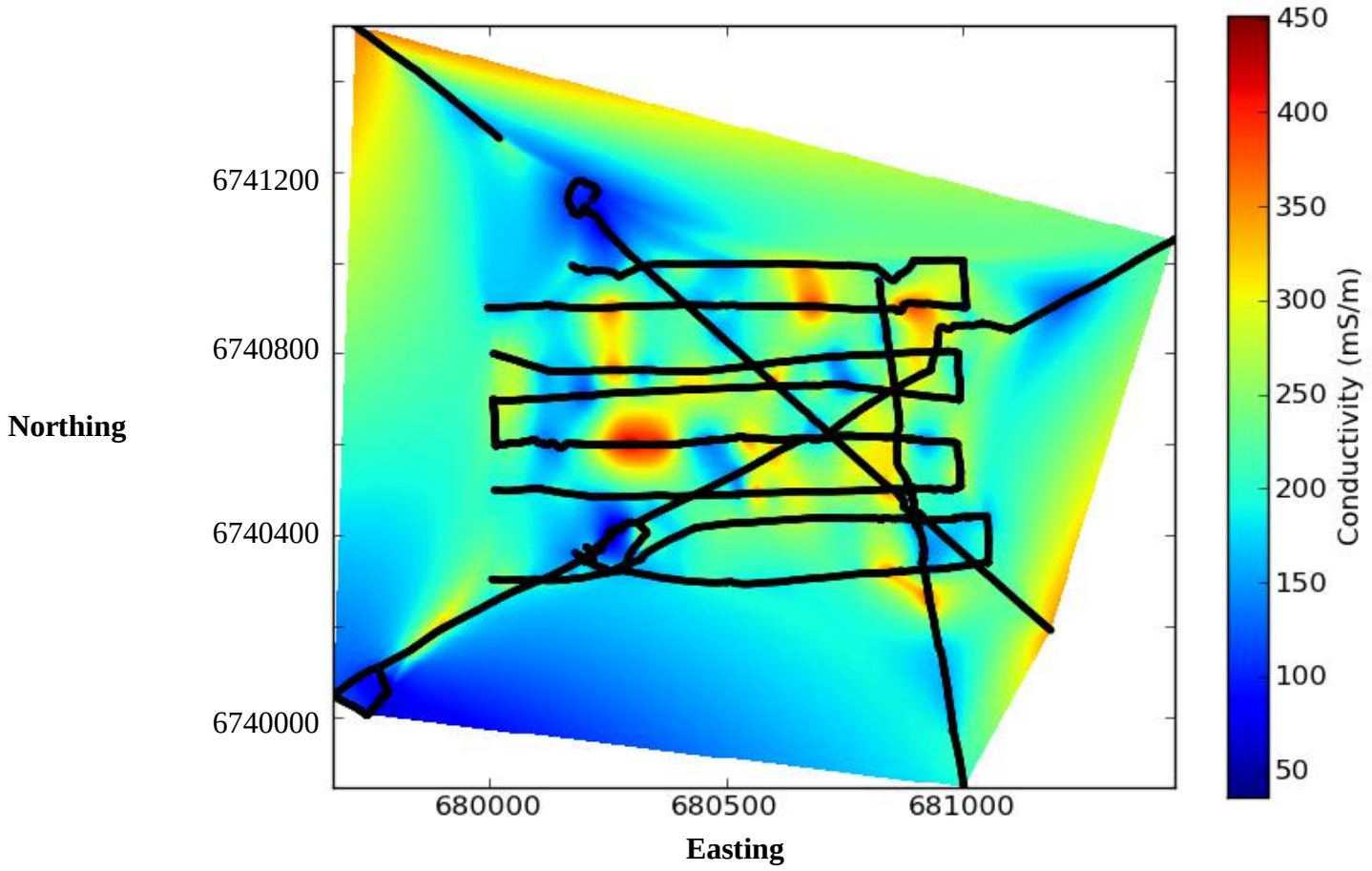
Northing
6741200
6740800
6740400
6740000
680000
680500
681000
Easting
450
400
350
300
250
200
150
100
50
Conductivity (mS/m)

Figure 13:

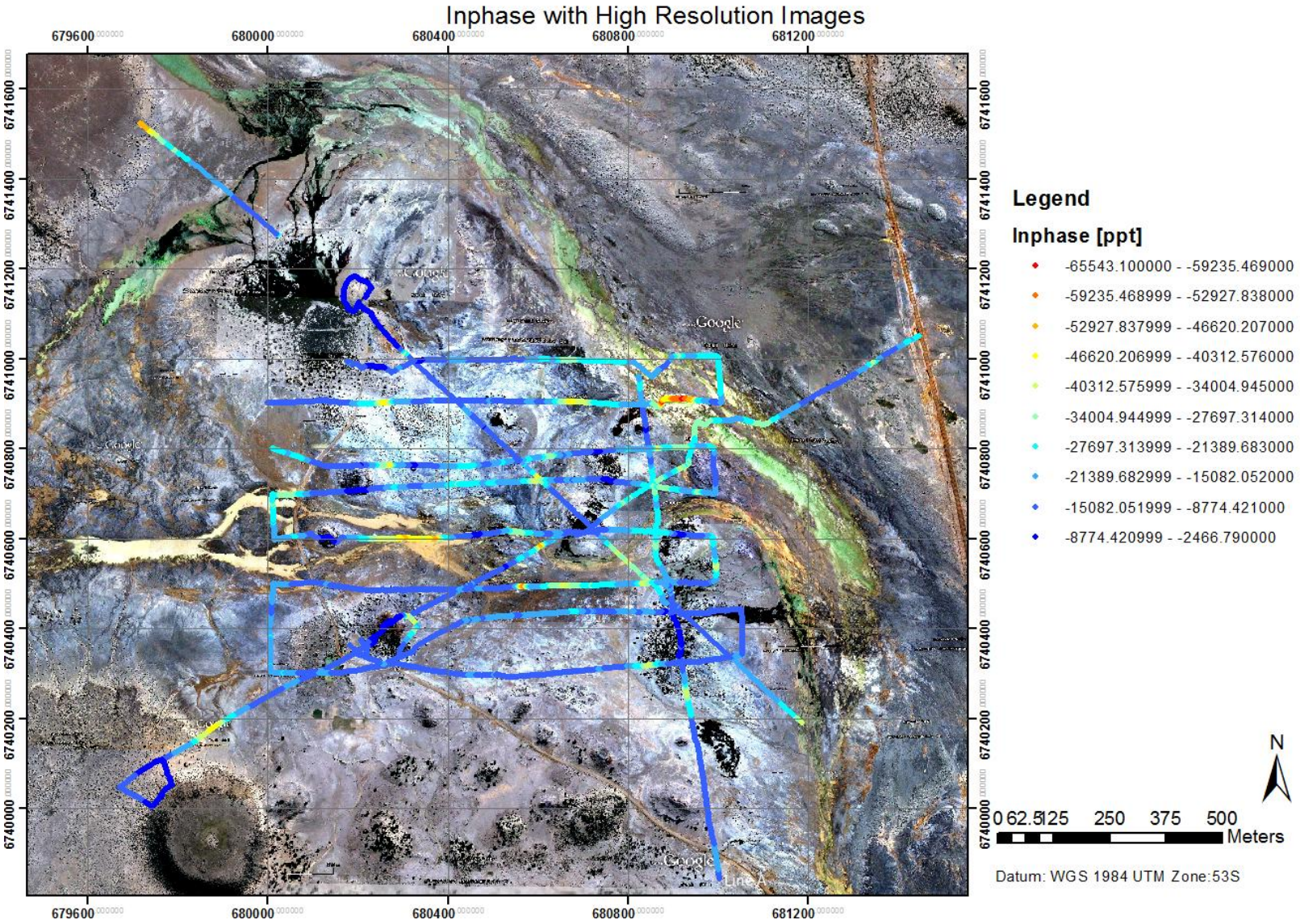
Inphase with High Resolution Images
679600
680000
680400
680800
681200
6741600
6741400
6741200
6741000
6740800
6740600
6740400
6740200
6740000
Legend
Inphase [ppt]
-65543.100000 - -59235.469000
-59235.468999 - -52927.838000
-52927.837999 - -46620.207000
-46620.206999 - -40312.576000
-40312.575999 - -34004.945000
-34004.944999 - -27697.314000
-27697.313999 - -21389.683000
-21389.682999 - -15082.052000
-15082.051999 - -8774.421000
-8774.420999 - -2466.790000
N
0 62.5 125 250 375 500
Meters
Datum: WGS 1984 UTM Zone:53S

Figure 14:

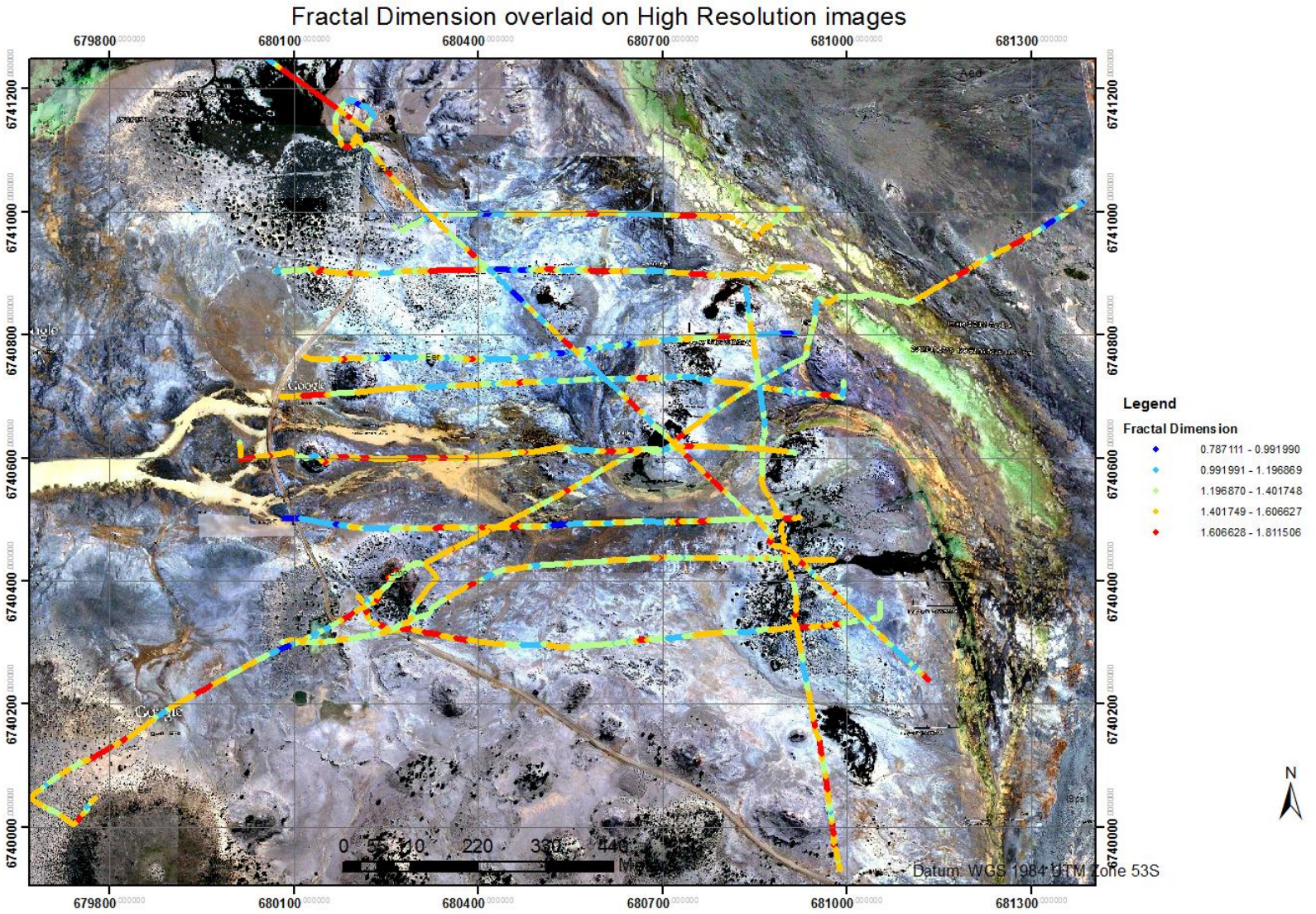
Fractal Dimension overlaid on High Resolution images
679800
680100
680400
680700
681000
681300
6741200
6741000
6740800
6740600
6740400
6740200
6740000
Legend
Fractal Dimension
0.787111 - 0.991990
0.991991 - 1.196869
1.196870 - 1.401748
1.401749 - 1.606627
1.606628 - 1.811506
N
0 55 110 220 330 440
Meters
Datum: WGS 1984 UTM Zone 53S

Figure 15:

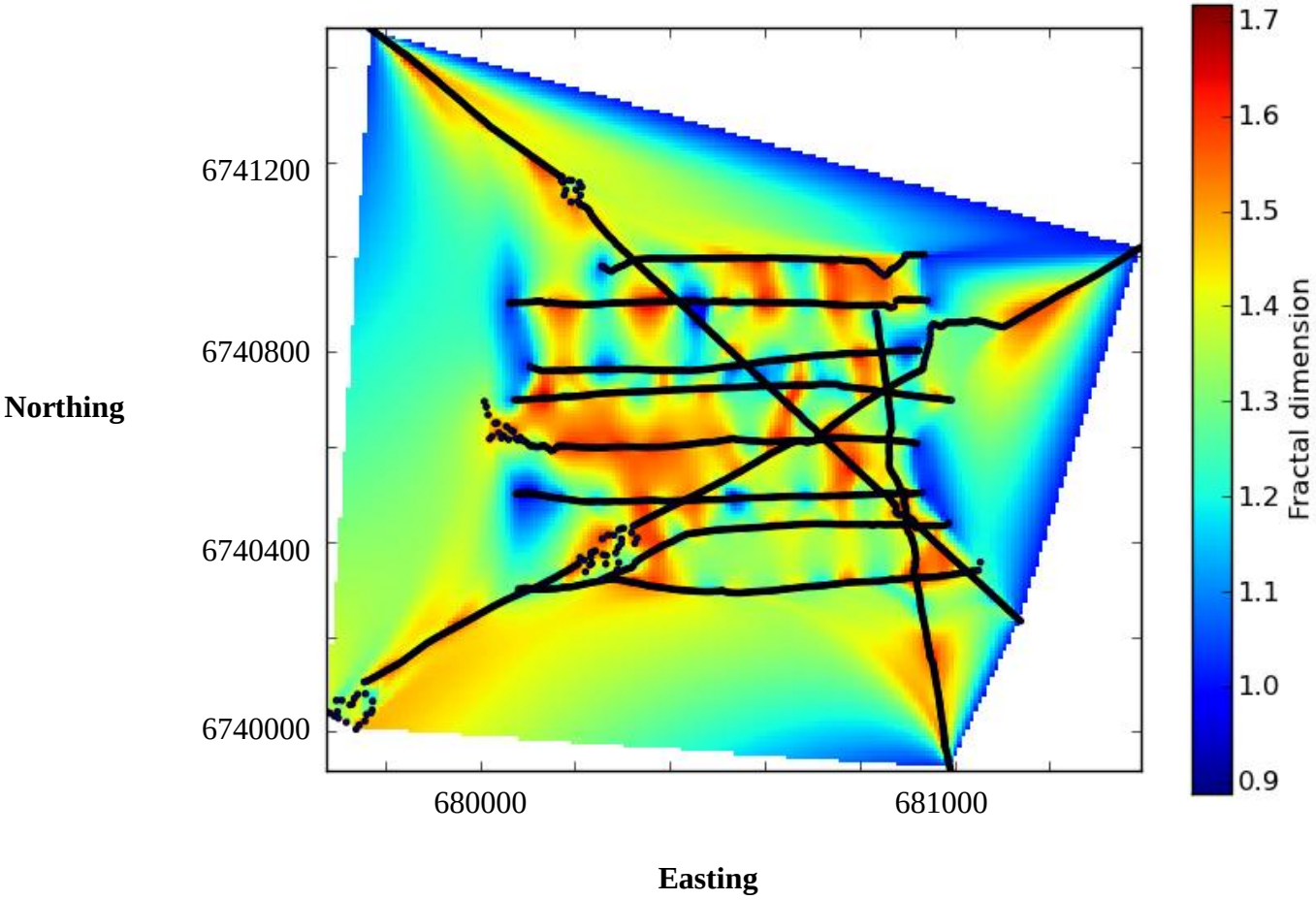
Northing
6741200
6740800
6740400
6740000
680000
681000
Easting
1.7
1.6
1.5
1.4
1.3
1.2
1.1
1.0
0.9
Fractal dimension

Figure 16:

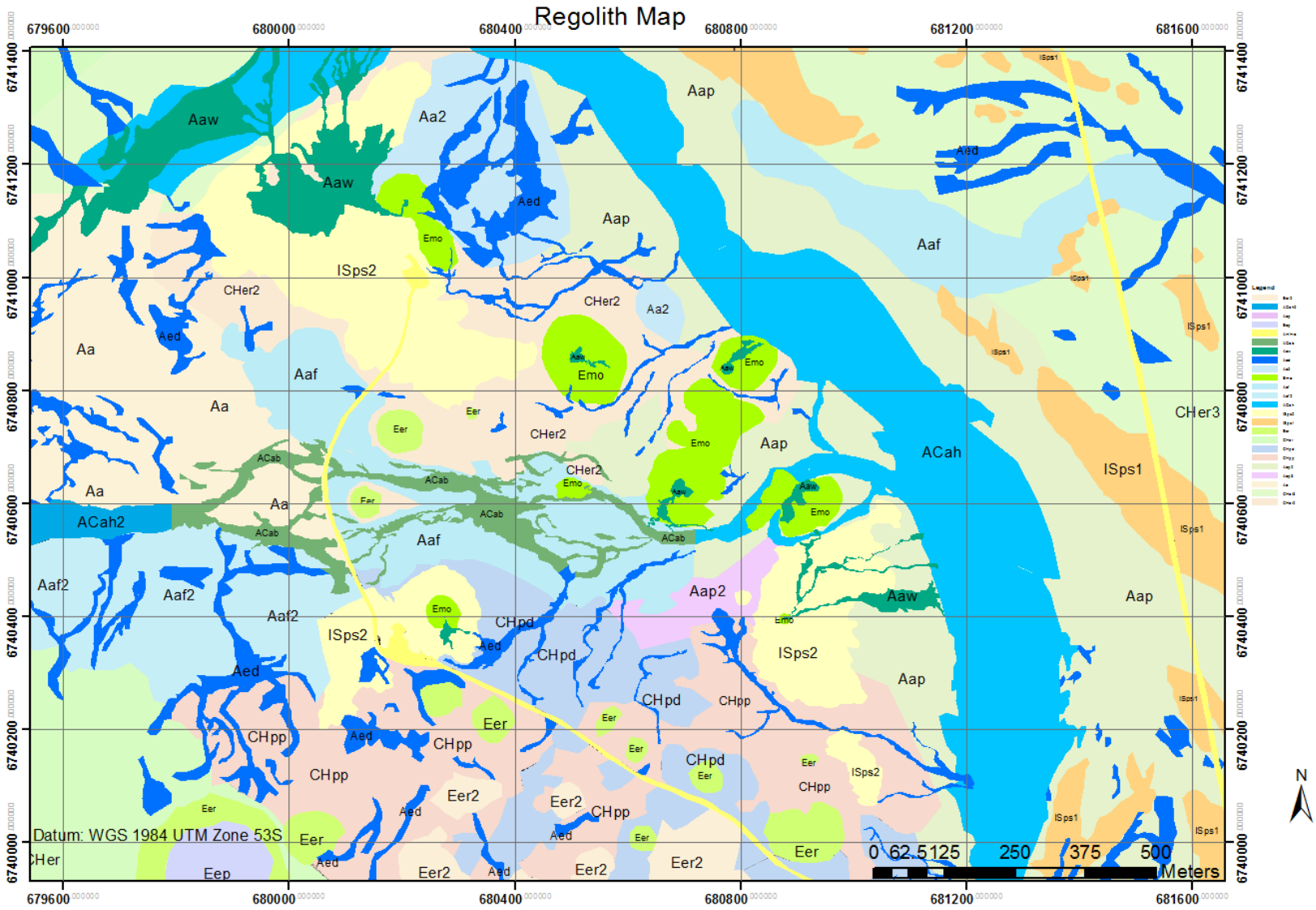
Regolith Map
679600
680000
680400
680800
681200
681600
6741400
6741200
6741000
6740800
6740600
6740400
6740200
6740000
Aaw
Aa2
Aap
Aed
Emo
ISps2
CHer2
Aa
Aaf
Eer
ACab
ACah2
Aaf2
CHpd
CHpp
Eer2
Eep
CHer
ACah
ISps1
CHer3
Datum: WGS 1984 UTM Zone 53S
0 62.5125 250 375 500
Meters
N

Figure 17:

Regolith Landform Legend :

Aa	**Alluivual sediments; alluvial landforms -** Alluvial sediments associated with the water movement of the surface runoff and meteoric water, as opposed to that of the springs. Areas of lag, with greater content of sand, compared to clay. Some salt precipitation.
Aa 2	**Alluivual sediments; alluvial landforms -** Alluvial landforms associated with The Bubbler, former area of runoff before build up altered the flow path of the spring. Build of carbonates and precipitates from the groundwater.
Aap	**Alluvial sediments; alluvial plain** - Alluvial sediments associated with The Bubbler runoff and drainage channel. Some depressions with increased amount of quartz lag. Some areas with sparse vegetation – such as grasses. More sand than clay.
Aap 2	**Alluvial sediments; alluvial plain -** Alluvial sediments associated with the lower lying area next to the slightly raised mound spring, as well as the braided alluivial channels running through the area. Increase in salt precipitation, contains some vegetation, groundcover bushes on small sand mound**s.**
Aaf	**Alluvial sediments, flood plain** - Flat area, characterised by hard, 'crusted' top layer of soil, large quartz lag – rounded. Slightly lower than surrounding areas.
Eep	**Evaporite erosional plain** - Top of Hamilton Hill, an extinct spring which is about 30m above the landscape. The top of the Hill is quite flat, and has some sparse vegetation.
Eer	**Evaporite erosional rise - Extinct springs** – which are up to 15m above the landscape. Some contain areas of reeds at the top of the mound – an indication of a previous fluid outlet. Springs themselves are comprised of precipitates from the groundwater, carbonates. An extinct spring can be differentiated from other rises within the landscape by the lack of vegetation to the sides and along the top of the spring itself, except for the reeds which, in most cases, still grow where the pool and source of moisture was previously.
Eer 2	**Evaporite erosional rise** - Vegetated sandy rises in the landscape. Not as high as the springs, but not characterised like the extinct or active springs with the lack of vegetation on the mound, bar from reeds where there is still some moisture. Vegetation is medium to large scrubby bushes, natives (sp.?). Prominent feature within the landscape but not the same as the springs.
Emo	**Evaporite mound spring** - Active mound springs, some of which, such as Blanche Cup and The Bubbler are raised up to 10 meters above the landscape. These are characterised by a pool at the centre of the spring, and surrounded by a mound of carbonate, or sandy clay, depending on the relative age of the springs. The Bubbler, Blanche Cup and several of the other, more dominant mound springs in the landscape have significant carbonate build up around the pool of the mound. The pool at the centre of the spring is generally populated by reeds.
CHpp	**Colluvial sediments, playa plain** - Vegetation free, low lying flat area, with areas alternating in clay and sand content. Precipitated salt 'nodules' on the surface, some clasts of sandstones or other types of rocks. Mudcracks in some areas indicate higher clay content in that area intermingled with areas of higher sand content. - Vegetation free, low lying flat area, with areas alternating in clay and sand content. Precipitated salt 'nodules' on the surface, some clasts of sandstones or other types of rocks. Mudcracks in some areas indicate higher clay content in that area intermingled with areas of higher sand content.

Aaf2	**Alluvial sediments, flood plain** - Flat area to the south of the large alluvial channel running through the area, characterised by lower lying basin type structures. Lag and slightly larger than pebble sized clasts dominate in the slightly lower area.
Aaw	**Alluval sediments, alluvial swamp** - Discharge from springs. Most areas characterised by consistently wet conditions, reed and grass growth; saturated soil, higher clay to sand ratio.
ACab	**Alluvial channel braided** - Contains some palaeochannels from the extinct springs? Otherwise from meteoric sources and surface runoff. Depressions in the landscape, most areas didn't contain any water, however one area which did; higher clay content to the top soil. Lag, smaller than that contained within the alluvial plains.
ACah	**Alluvial channel deposits; alluvial channel** - The main area of The Bubbler discharge and outflow. Some of the water in this area is from the collection of rainwater. Areas of carbonate build up from the spring water precipitates. Some areas with lag and larger pebble sized lag cemented into carbonate.
ACah 2	**Alluvial channel deposits; alluvial channel** - Alluvial channel that leads into the braided area, meteoric sources and surface runoff being the feeder.
Aed	**Alluvial sediment drainage depressions** - Areas in the landscape characterised by being slightly lower than the surrounding areas, and thus are the preferential path for surface runoff. The majority of the drainage depressions have slightly higher clay content. These areas also corresponded with a grey-green, possibly smectictic, clay about 2-3cm under the top layer of the surface.
Cher	**Colluivial sediments; erosional rise** - Sandy, vegetated area to the west of Hamiliton Hill; Higher than surrounding landscape which are alluvial depressions. Vegetation only up to 1m high, and not dense. There is less lag and more influence from the erosional of the mound spring directly to the east.
Cher 2	**Colluivial sediments; erosional rise** - Area surrounding The Bubbler, which has less of an association with alluvial processes. Some areas of vegetation with some small shrubs, and varying compositions of sandy and clay; most of the area has a high amount of precipitated salt on the surface.
CHpd	C**olluvial sediments; depositional plain** - Areas around the smaller extinct springs, that have varying compositions of sand to clay. These areas include small 'mounds' (less than 1m) with vegetation, such and reeds and grasses, mounds tend to be of a high sand content, most likely Aeolian derived.
ISps 1	**Aeolian Sand – sand plain** - Sand dunes/banks on the east side of The Bubbler runoff. Up to 3-4 meters above the depression in which the alluvial channel of The Bubbler runoff flows through. Higher sand content and lower clay. The vegetation is small (less than .5m in height) shrubs and grasses.
ISps 2	**Aeolian Sand – sand plain** - Sand dunes around the active springs. Lower clay content, sands aeolian in origin. These areas can the majority of the vegetation that is found in the landscape. Some sandy areas have medium to dense vegetation generally towards the spring with density thinning as the springs radiated outward.
M-	Dirt road/track into the National Park and the car parks at The Bubbler and Blanche Cup are the main anthropogenic effects on the area.

Figure 18:

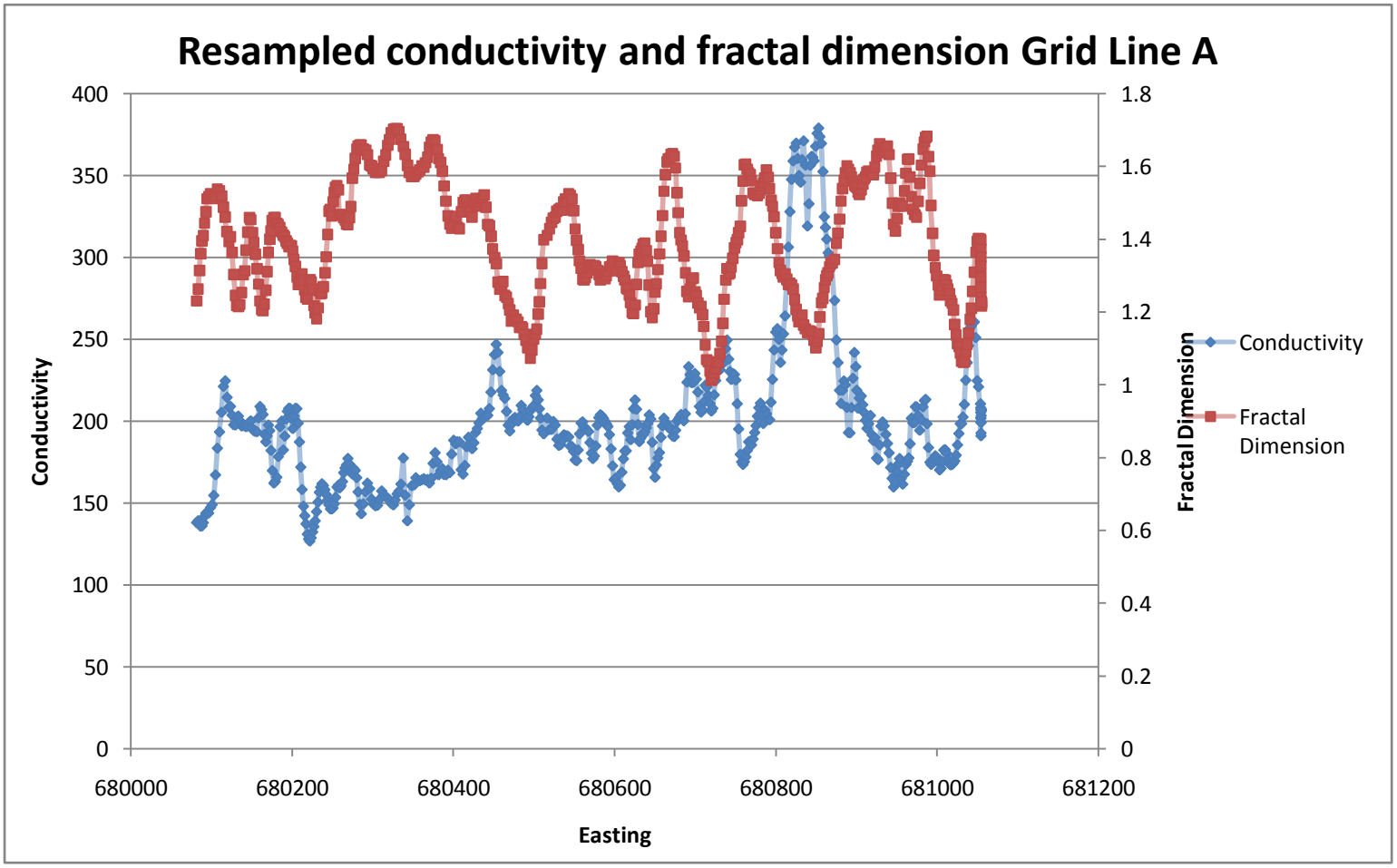
Resampled conductivity and fractal dimension Grid Line A
Conductivity
Fractal Dimension
Easting
400
350
300
250
200
150
100
50
0
1.8
1.6
1.4
1.2
1
0.8
0.6
0.4
0.2
0
680000
680200
680400
680600
680800
681000
681200
Conductivity
Fractal Dimension

Figure 19:

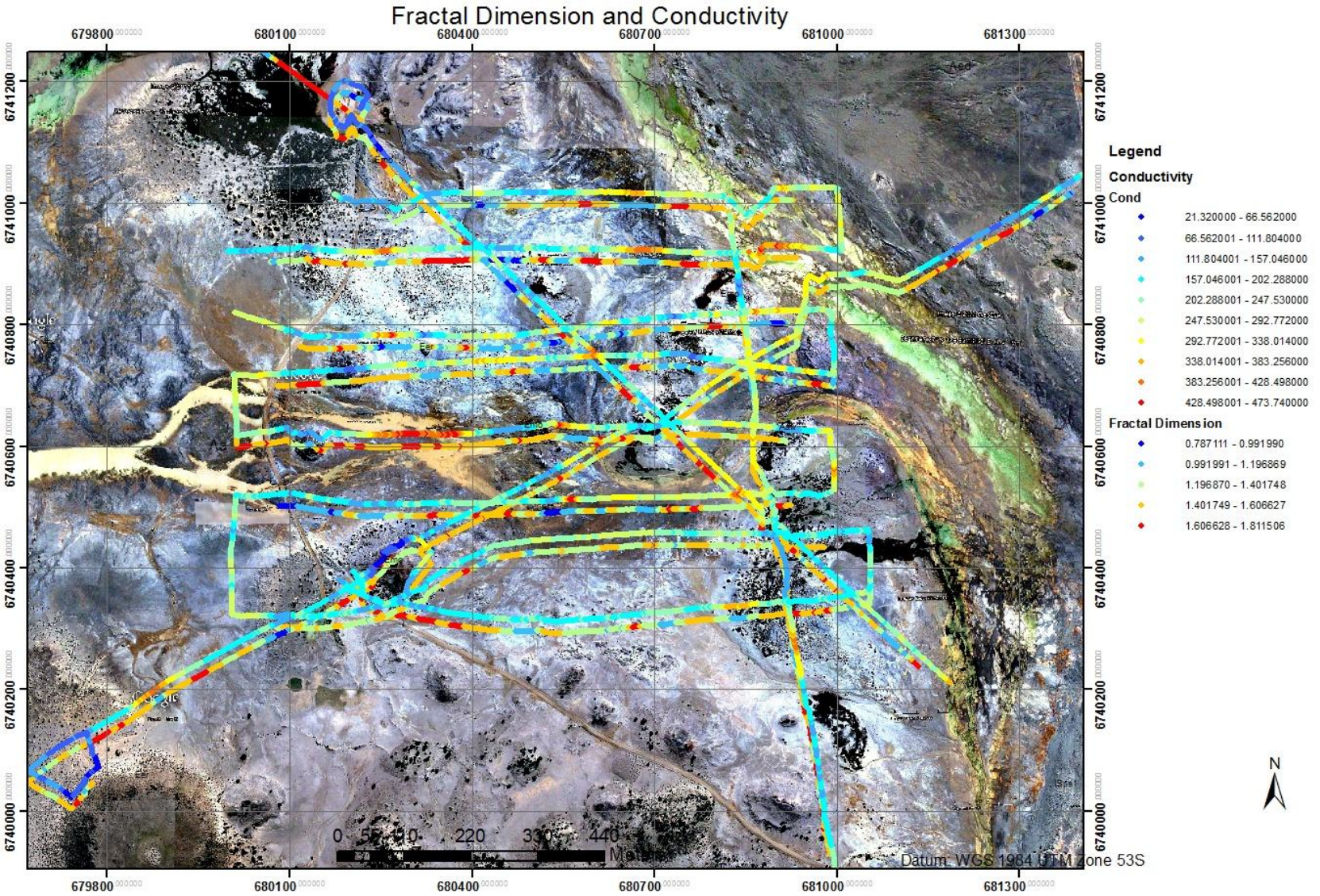
Fractal Dimension and Conductivity
679800
680100
680400
680700
681000
681300
6741200
6741000
6740800
6740600
6740400
6740200
6740000
Legend
Conductivity
Cond
21.320000 - 66.562000
66.562001 - 111.804000
111.804001 - 157.046000
157.046001 - 202.288000
202.288001 - 247.530000
247.530001 - 292.772000
292.772001 - 338.014000
338.014001 - 383.256000
383.256001 - 428.498000
428.498001 - 473.740000
Fractal Dimension
0.787111 - 0.991990
0.991991 - 1.196869
1.196870 - 1.401748
1.401749 - 1.606627
1.606628 - 1.811506
0 55 110 220 330 440
Meters
N
Datum: WGS 1984 UTM Zone 53S

Figure 20:

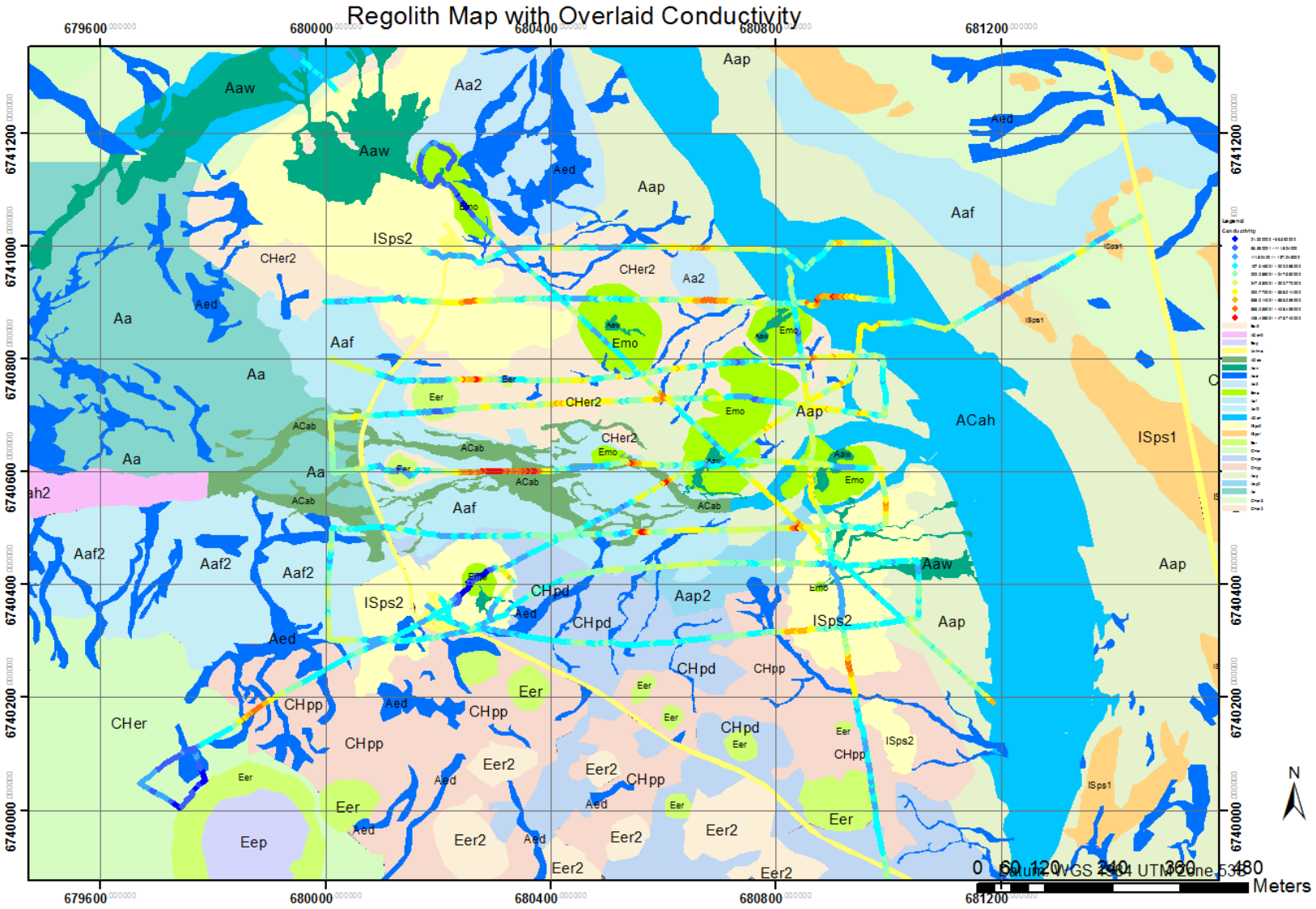
Regolith Map with Overlaid Conductivity
679600
680000
680400
680800
681200
6741200
6741000
6740800
6740600
6740400
6740200
6740000
Aaw
Aa2
Aap
Aed
Aaf
ISps2
CHer2
Aa
Emo
Eer
ACab
ACah
ISps1
Aaf2
CHpd
Aap2
CHpp
CHer
Eer2
Eep
N
0 60 120 240 360 480
Meters

Figure 21:

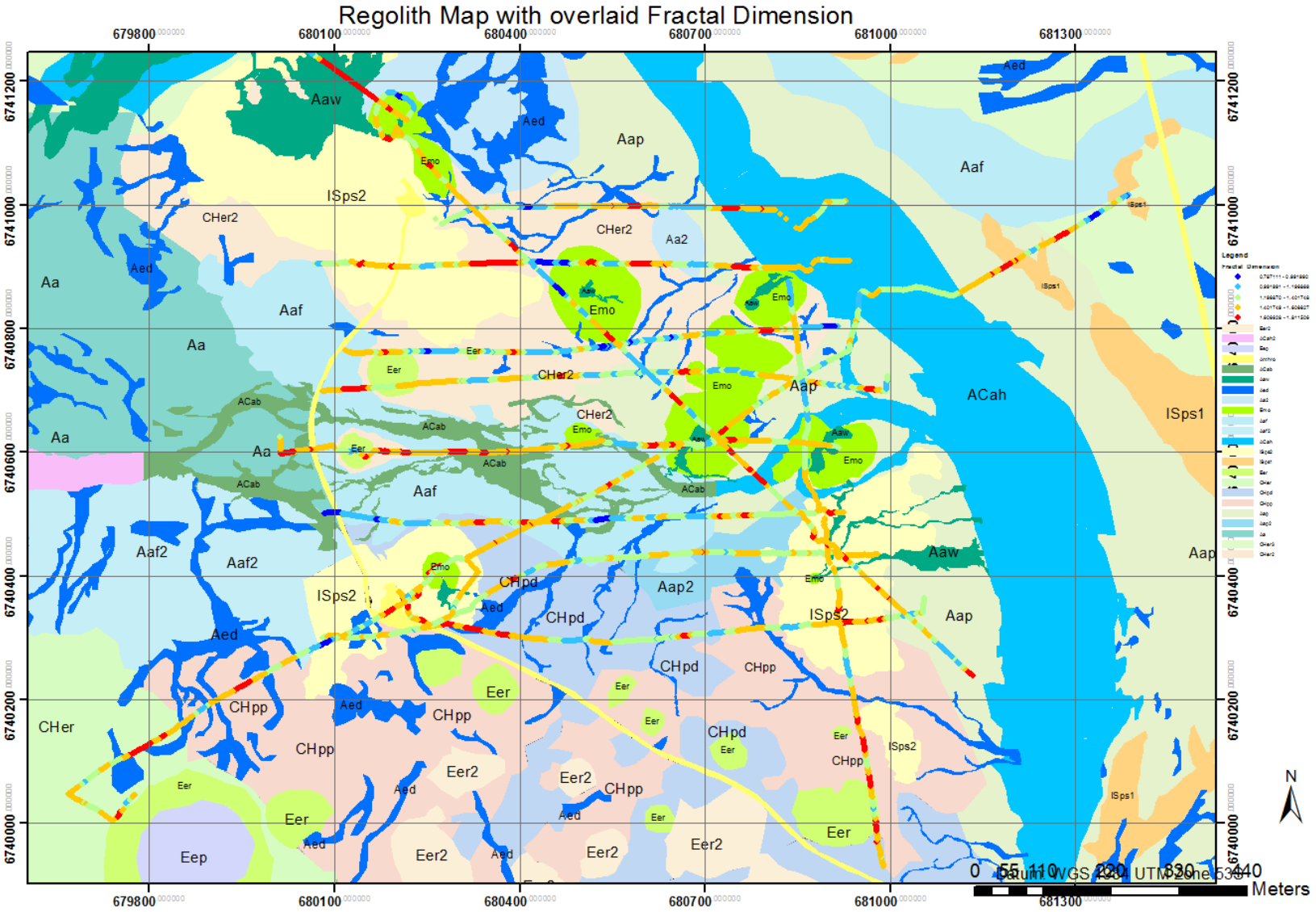
Regolith Map with overlaid Fractal Dimension
679800
680100
680400
680700
681000
681300
6741200
6741000
6740800
6740600
6740400
6740200
6740000
Aaw
Aed
Aap
Aaf
ISps2
CHer2
Aa2
Aa
Emo
Eer
ACab
Aaf2
CHpd
CHpp
Eer2
Eep
CHer
ACah
ISps1
Legend
Fractal Dimension
0 55 110 220 330 440
Meters
N
Datum: WGS 1984 UTM Zone 53N

Figure 22:

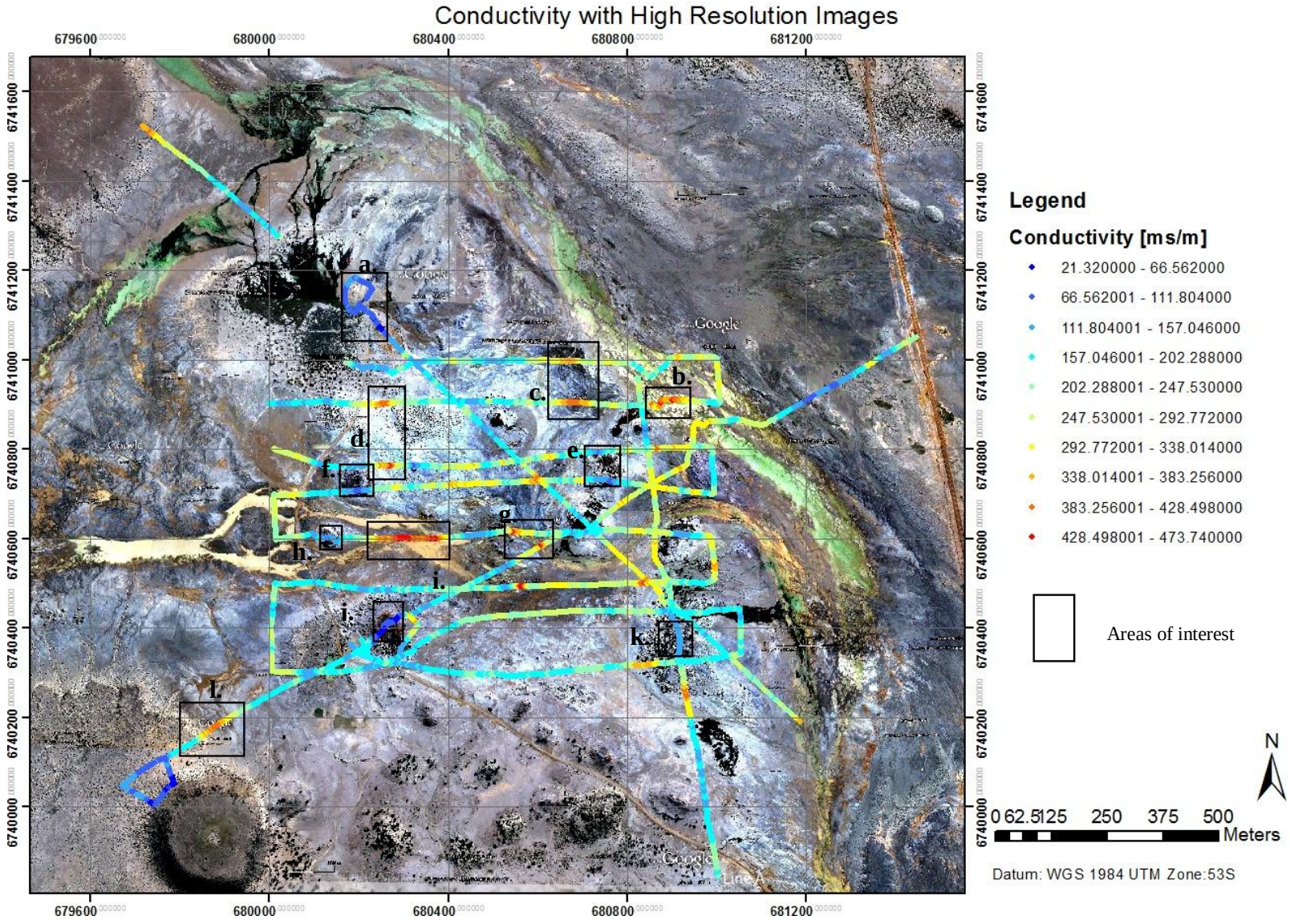
Conductivity with High Resolution Images
679600
680000
680400
680800
681200
6741600
6741400
6741200
6741000
6740800
6740600
6740400
6740200
6740000
a.
b.
c.
d.
e.
f.
g.
h.
i.
j.
k.
l.
Legend
Conductivity [ms/m]
21.320000 - 66.562000
66.562001 - 111.804000
111.804001 - 157.046000
157.046001 - 202.288000
202.288001 - 247.530000
247.530001 - 292.772000
292.772001 - 338.014000
338.014001 - 383.256000
383.256001 - 428.498000
428.498001 - 473.740000
Areas of interest
N
0 62.5125 250 375 500
Meters
Datum: WGS 1984 UTM Zone:53S

Figure 23:

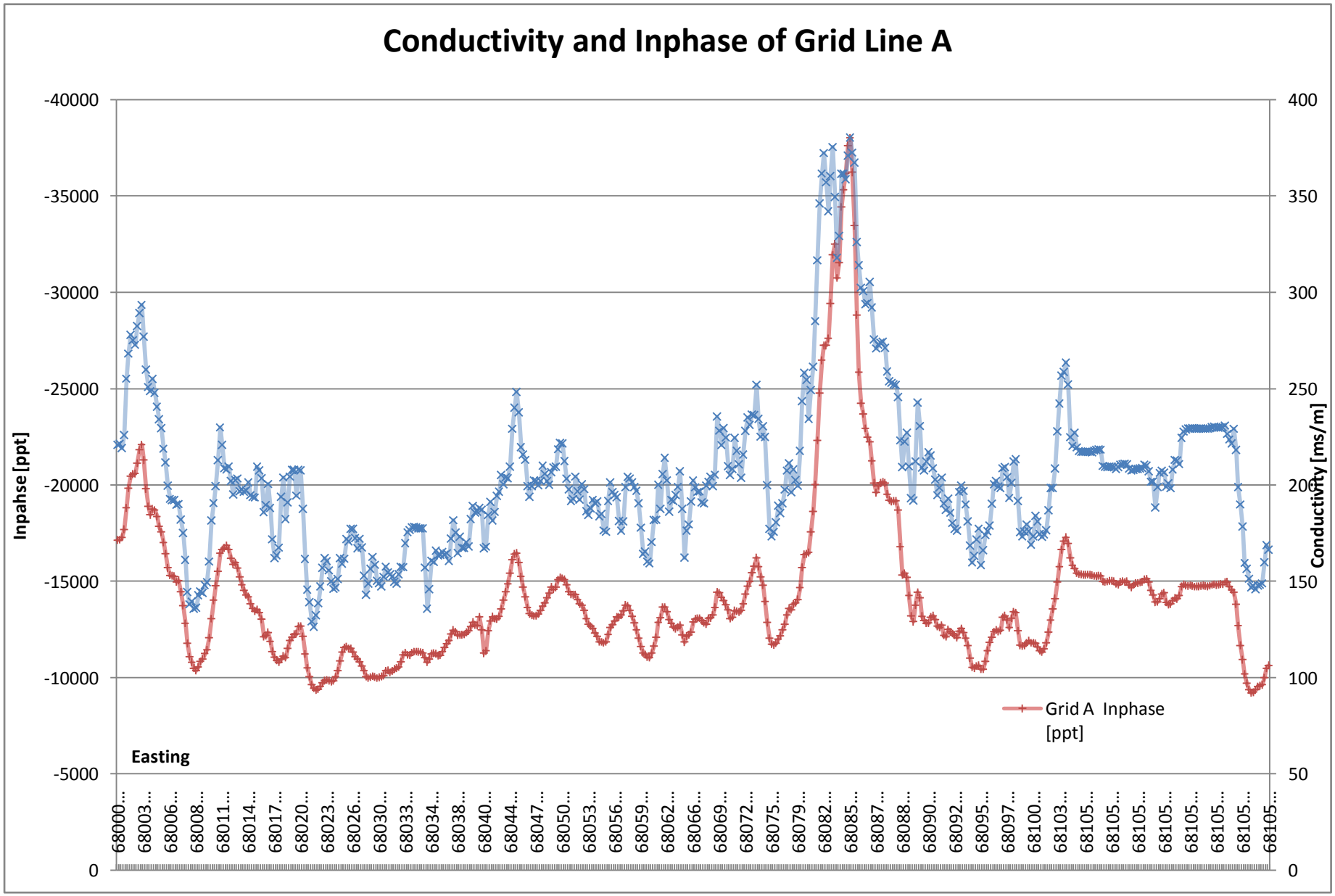
Conductivity and Inphase of Grid Line A
Inpahse [ppt]
Conductivity [ms/m]
-40000
-35000
-30000
-25000
-20000
-15000
-10000
-5000
0
400
350
300
250
200
150
100
50
0
Grid A Inphase [ppt]
Easting
68000...
68003...
68006...
68008...
68011...
68014...
68017...
68020...
68023...
68026...
68030...
68033...
68034...
68038...
68040...
68044...
68047...
68050...
68053...
68056...
68059...
68062...
68066...
68069...
68072...
68075...
68079...
68082...
68085...
68087...
68088...
68090...
68092...
68095...
68097...
68100...
68103...
68105...
68105...
68105...
68105...
68105...
68105...
68105...

Figure 24:

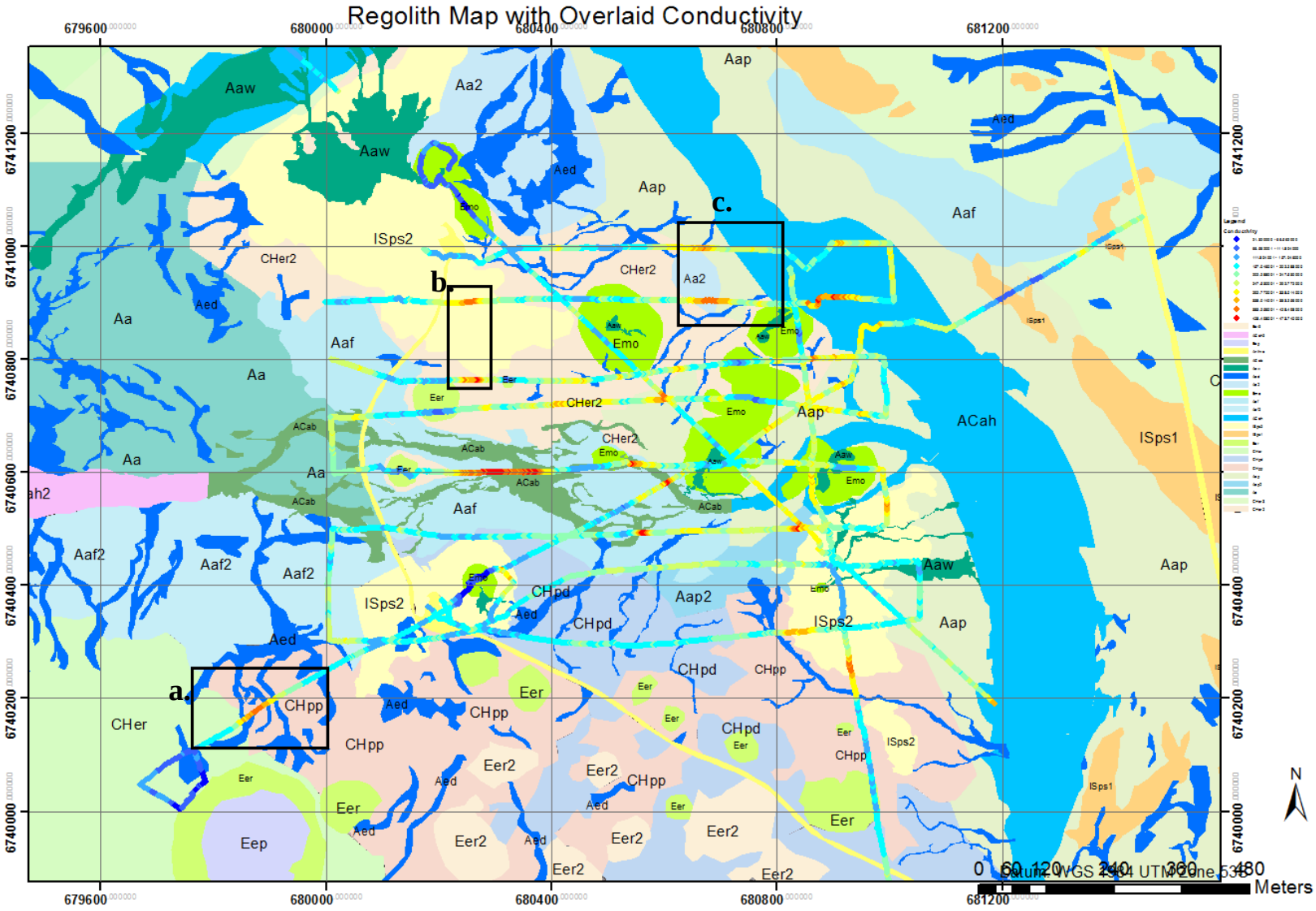
Regolith Map with Overlaid Conductivity
679600
680000
680400
680800
681200
6741200
6741000
6740800
6740600
6740400
6740200
6740000
a.
b.
c.
Aaw
Aa2
Aap
Aed
Aaf
Aa
Emo
ISps2
CHer2
Eer
ACab
CHpd
Aap2
CHpp
Eer2
Eep
CHer
Aaf2
ah2
ACah
ISps1
N
0 60 120 240 360 480
Datum: WGS 1984 UTM Zone 53N
Meters

Figure 25:

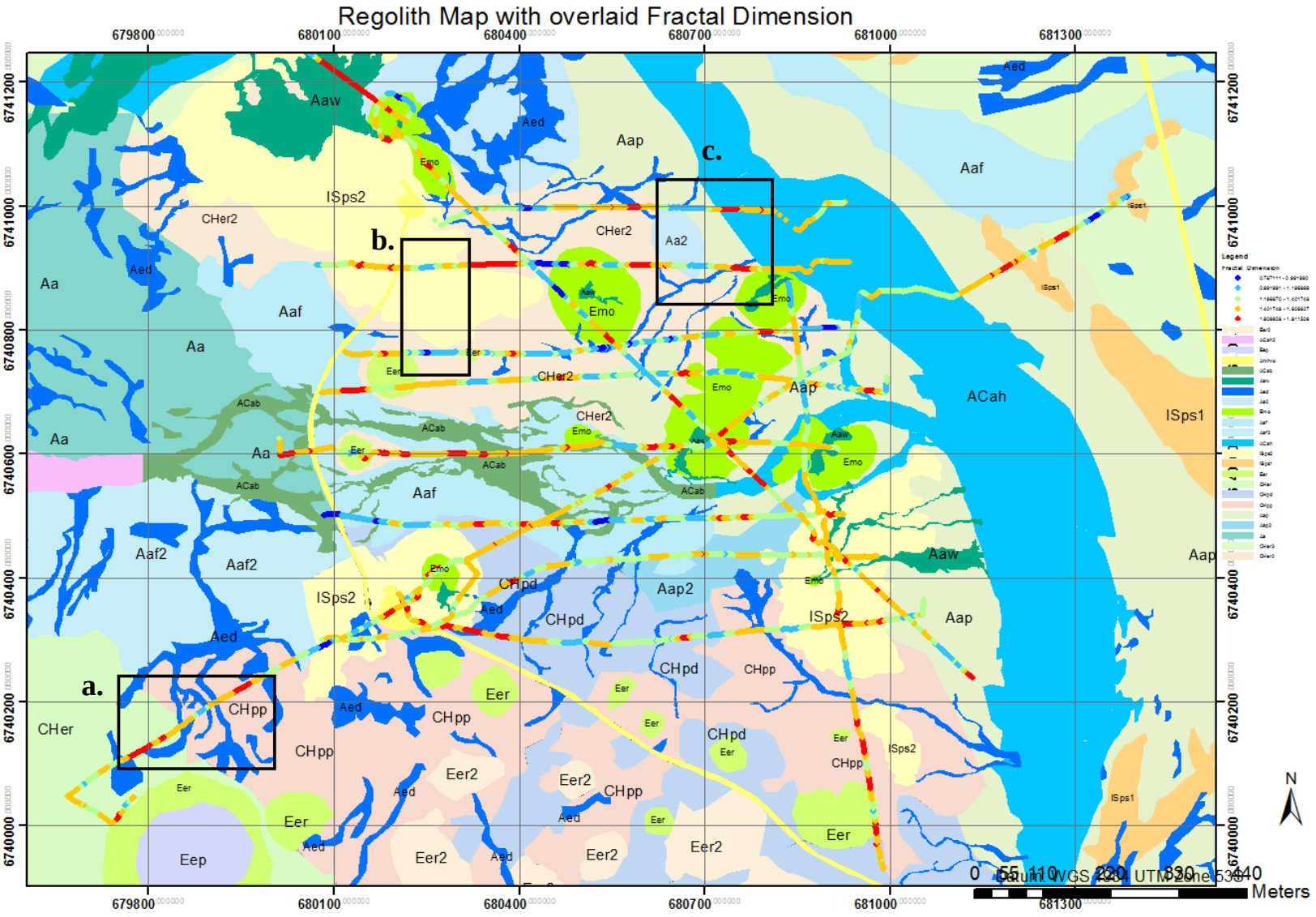
Regolith Map with overlaid Fractal Dimension
679800
680100
680400
680700
681000
681300
6741200
6741000
6740800
6740600
6740400
6740200
6740000
a.
b.
c.
Aaw
Aed
Aap
Aaf
Aa
Aa2
ISps2
ISps1
CHer2
Emo
ACah
ACab
Aaf2
Aap2
CHpd
CHpp
CHer
Eer
Eer2
Eep
N
0 55 110 220 330 440
Meters

Figure 26:

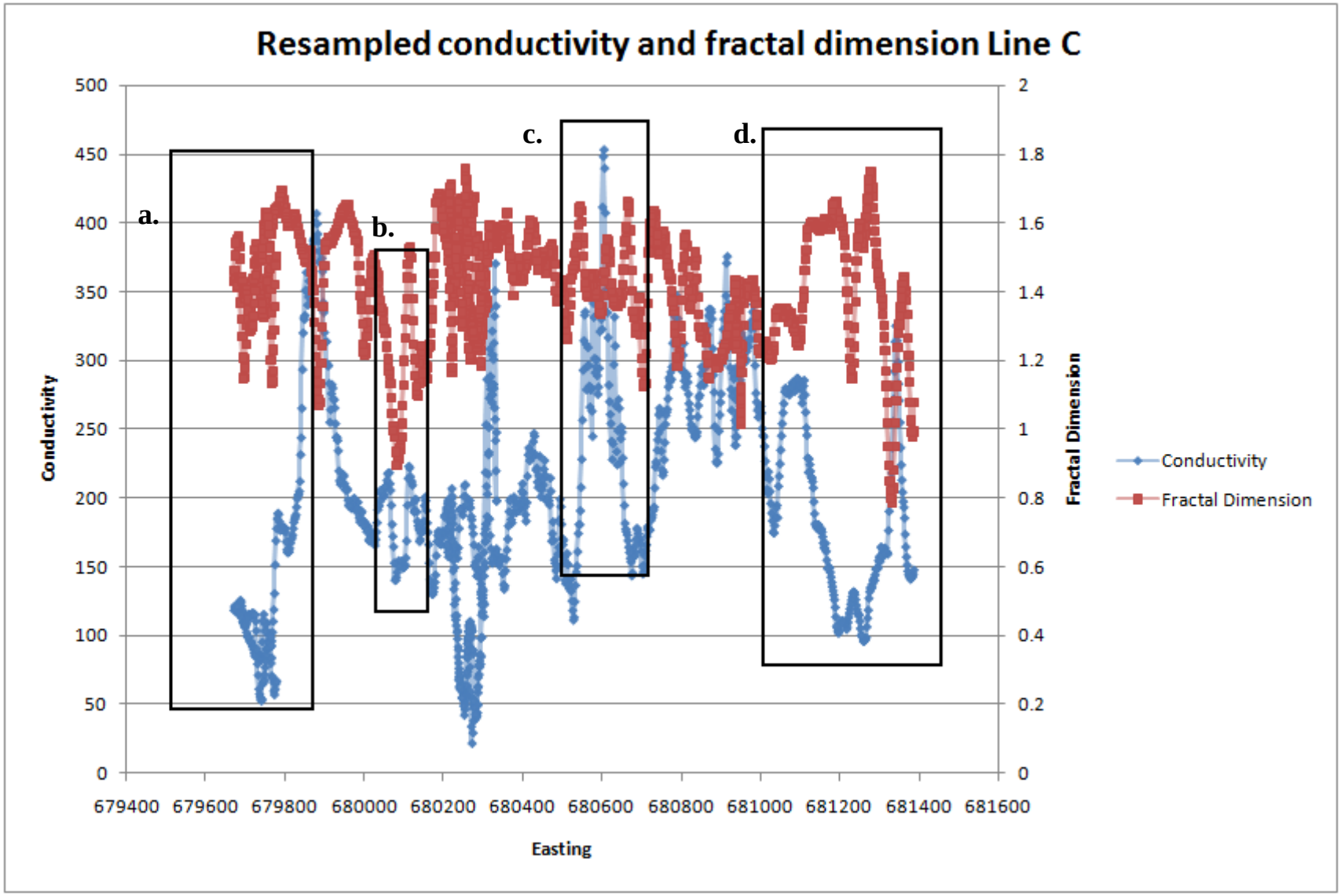
Resampled conductivity and fractal dimension Line C
a.
b.
c.
d.
Conductivity
Fractal Dimension
Easting
Conductivity
Fractal Dimension
500
450
400
350
300
250
200
150
100
50
0
2
1.8
1.6
1.4
1.2
1
0.8
0.6
0.4
0.2
0
679400
679600
679800
680000
680200
680400
680600
680800
681000
681200
681400
681600